means of Student *t*-test. Results are reported as mean ± standard deviation.

RESULTS

Summary of Clinical Features

All the pedigrees studied are shown in Figure 1 and clinical data of 11 patients (m:f = 8:3; 48.5 ± 11.1 years) are presented in Table 1 (detailed clinical information is provided as supplementary data). All 11 patients harbored *SNCA* duplication and presented with parkinsonism consisting mostly of rigidity and bradykinesia, tremor being less prominent. Two patients had slight tremor, five patients had no tremor. Three patients (B-II-7, E-III-4, and F-III-2) had dementia with MMSE (mini-mental state examination) scores under 20. The clinical features of these three patients were consistent with a clinical diagnosis of PD with dementia (PDD); patients with a disease duration <10 years had milder parkinsonism. Parkinsonism was the initial symptom in all (n = 11). Two patients (B-II-7 and E-III-4) had severe disease with a Hoehn and Yahr stage V. In the subsequent clinical course, six patients developed hallucinations and/or delusions and three patients (A-II-9, A-II-11, and F-III-2) had severe depression. Disease penetrance among carriers was age-associated and a lifetime estimate of overall penetrance in seven families was 43.8%.

Genomic Analysis of *SNCA* Duplication

Haplotypes were constructed using five microsatellite markers in the *SNCA* region (Fig. 1). Analysis indicates three possible independent allele sharing for (1) Family A and F, (2) Family B and C, and (3) Family D and G. No allele sharing was observed for Family E suggesting a de novo event (Fig. 1). Real time PCR analysis showed that two pedigrees (Family A and F) had a duplication of the *SNCA* locus and only a part of the *MMRN1* gene (supplementary Fig. 1); whereas the other families studied had a duplication of the *SNCA* locus and the entire *MMRN1* gene. The Affymetrix SNP 250K array confirmed the results of quantitative PCR. Family E had the smallest duplicated region (0.2Mb) including the *SNCA* locus (Fig. 2). All patients were negative for *PARKIN*, *PINK1*, or *DJ-1* mutations.

PET Studies

Our four patients with a *SNCA* duplication showed severe reductions of dopamine transporters in the anterior and posterior putamen and caudate by [^{11}C]-CFT PET. *P*-values were < 0.05 between asymptomatic carriers, PD with Hoehn and Yahr stage III, and normal controls subjects (Table 2 and Fig. 3A). [^{11}C]-CFT PET showed a more severe reduction of dopamine transporters in patients with *SNCA* duplication compared to sporadic PD patients, although both groups had the same Hoehn and Yahr stage III: caudate (P = 0.001), anterior putamen (P = 0.001), and posterior putamen (P = 0.001).

On [^{11}C]-RAC PET, dopamine D_2 receptor density was overall similar to normal controls. However, interestingly, we observed a severe reduction in D_2 receptor density in the caudate of patients with *SNCA* duplication [2.84 ± 0.15 (±SD)] compared to asymptomatic carriers (4.09 ± 0.25; P = 0.029), PD patients with Hoehn and Yahr stage III disease (4.45 ± 0.53; P = 0.001), and normal control subjects (4.46 ± 0.38; P = 0.003). Regarding the FDG-PET study, our results showed significantly reduced glucose metabolism in the parieto-temporo-occipital cortex bilaterally (Fig. 3B), the three asymptomatic carriers showed normal findings (data not shown).

REM Sleep Behavior Disorder

Only patient A-II-9 had RBD out of six patients with *SNCA* duplication examined. She experienced oneiric behavior while dreaming, and had REM sleep without atonia (RWA) on PSG, an important finding in the diagnosis of RBD.[26] Patient A-II-11 reported an experience of shouting, standing up and kicking in bed for a few minutes while sleeping. He was diagnosed as possible RBD because definite RWA was not observed on PSG. All three asymptomatic carriers did not report any abnormal behaviors during sleep and their PSGs were normal.

Olfactory Testing

The values for patients with *SNCA* duplication were OT; 2.25 ± 1.63, OD; 6.67 ± 2.58, and OI; 5.83 ± 3.19, for asymptomatic carriers OT; 6.9 ± 3.27, OD; 11.6 ± 1.82, and OI; 10.0 ± 4.95, and for normal controls OT; 7.67 ± 1.76, OD; 11.1 ± 2.33, and OI; 10.6 ± 1.79. The patients with *SNCA* duplication showed severe reduction in OT, OD, and OI compared to normal controls (P < 0.0005), and in OT and OD compared to asymptomatic carriers (P < 0.05). There were no differences between asymptomatic carriers and normal controls (P > 0.05; Fig. 3C).

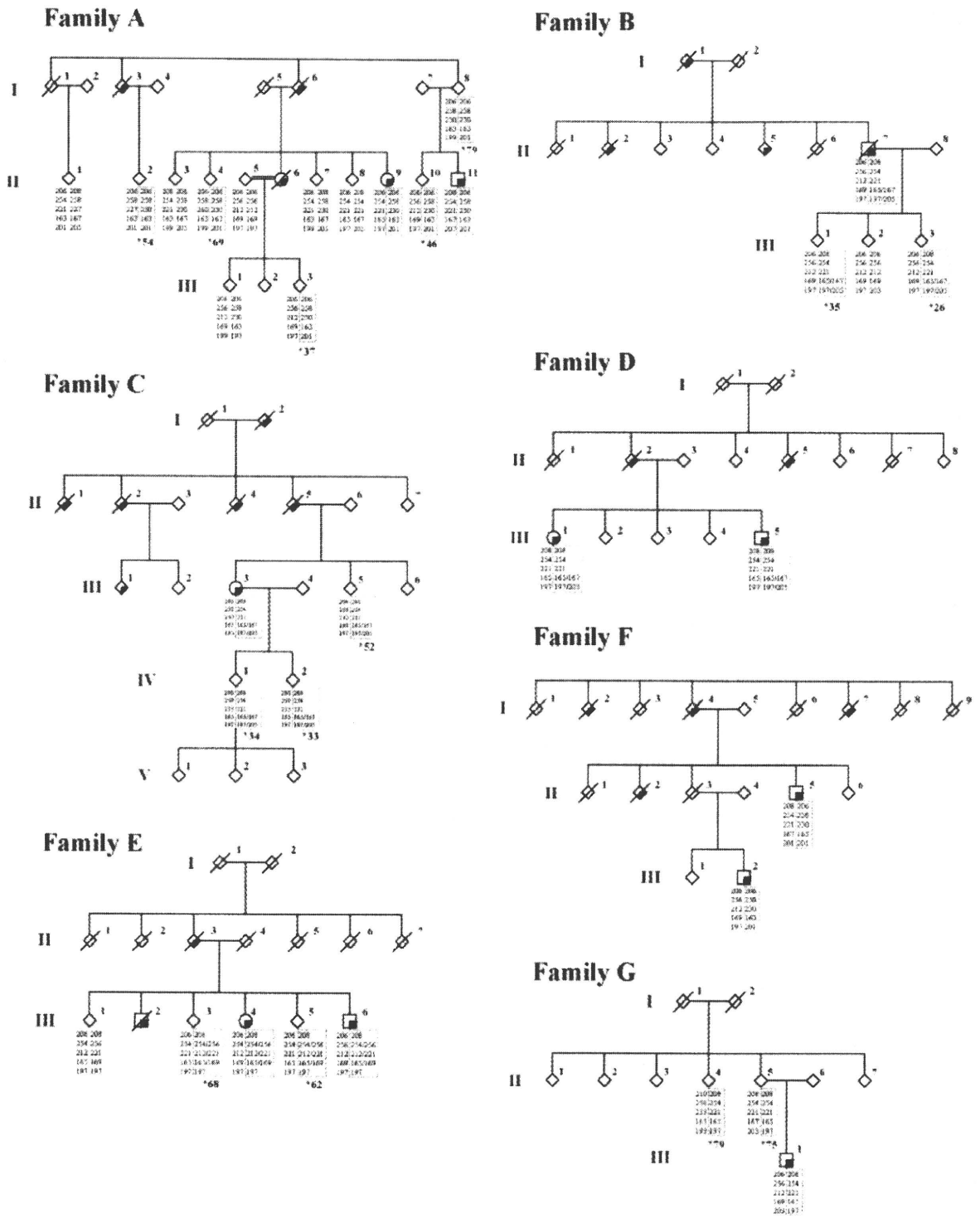

FIG. 1. Pedigrees of *SNCA* duplication families and haplotype analysis. The pedigrees with *SNCA* duplication are shown. Affected patients with parkinsonism are represented with a quarter-filled symbol and asymptomatic carriers with an asterisk with each age under genotyping results. Box with dot line around allele indicates duplicated allele. Families **A** and **F** (prefecture Nagano) and Families **B**, **C**, and **D** (prefecture Shizuoka) come from the same rural area of Japan. A-II-4, A-I-8, and G-II-5 were asymptomatic carriers older than 70 years of age. Haplotype markers (D4S3475, D4S3477, D4S3480, D4S3479, and D4S3474) in the *SNCA* region showed the possible existence of four founders in the seven duplication pedigrees of Japanese origin.

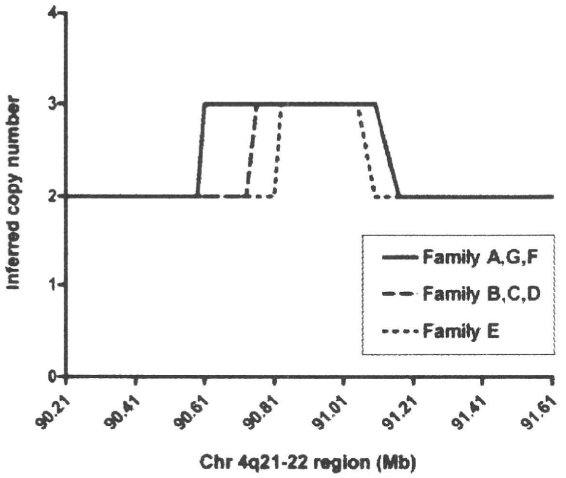

FIG. 2. Analysis of gene chip mapping 250K array. The assessment of copy number variation based on analysis of GeneChip Mapping 250K. Array data for chromosome 4q21, 90.21- to 91.61- Mb centromeric to telomeric. A value of 2.0 indicates normal diploid copy number. These results demonstrate three different regions and three copy numbers (monoallelic duplication). Patients A-II-9 and B-II-7 have been previously confirmed by this method and herein, C-III-3, D-III-5, E-III-6, F-III-2, and G-III-1 were examined.[12]

DISCUSSION

Herein, we describe four new *SNCA* duplication pedigrees and one apparent sporadic PD patient. In total, our *SNCA* duplication patients of Japanese ethnicity came from six pedigrees and one sporadic case. In addition, haplotype analysis of the seven families indicates four independent founder events (Fig. 1). All the duplicated regions in our families share the entire *SNCA* gene (Fig. 2), thus we hypothesize that multiple copies of *SNCA* alone can cause parkinsonism with or without dementia.

The average age of onset in *SNCA* duplication patients is 15 years older than that of *SNCA* triplication individuals suggesting that the copy number variation influences the clinical severity and the rate of progression.[27] Our study demonstrates that the clinical features of *SNCA* duplication vary even within the same family as seen in Family B, E, and F. Three patients developed dementia, whereas 14 persons did not show symptoms despite harboring a duplication of *SNCA*; age of onset ranged from 31 to 69 years (average 48.5 ± 11.2) in these families. Eight of the 11 patients

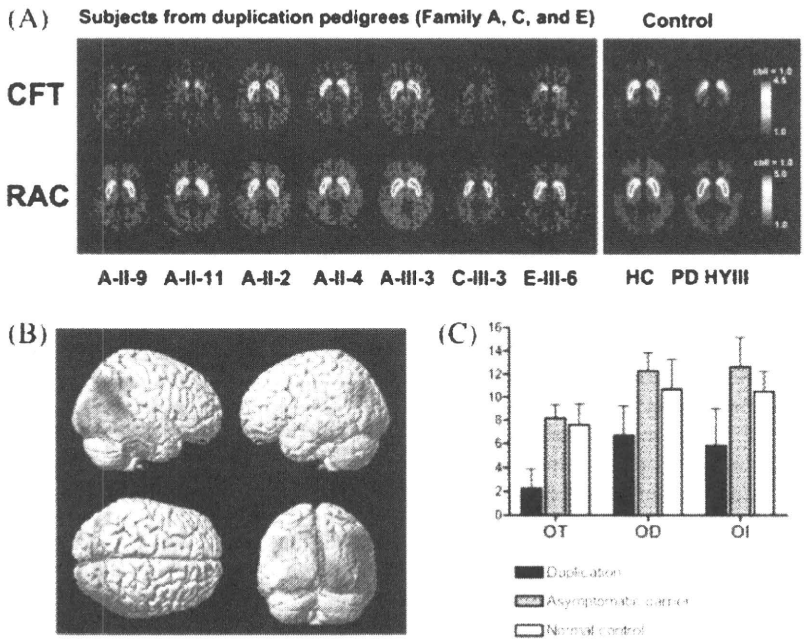

FIG. 3. PET study and olfactory testing. (**A**) The PET study of duplication patients was performed with CFT and RAC. A severe reduction of dopamine transporters was demonstrated in bilateral caudate and putamen at CFT in all affected patients. Asymptomatic carriers did not show any reduction in CFT and RAC. (**B**) FDG–PET. SPM was performed allowing exploratory voxel by voxel group comparisons throughout the entire brain volume ($P < 0.05$, k < 300). Four patients with *SNCA* duplication and 30 normal controls were evaluated. Significant reductions of FDG signal were localized in the occipital lobe of *SNCA* duplication patients (composite image of all four patients shown). (**C**) Olfaction was assessed by "Sniffin" sticks' (Burghardt, Wedel, Germany) for Olfactory Threshold (OT), odor Discrimination (OD), and odor Identification (OI). Five patients, five asymptomatic carriers (AC), and 22 normal controls (NC) were assessed. Reduced levels were seen in the patients with *SNCA* duplication in all OT, OD, and OI, as opposed to NC and AC.

(72.7%) had a good response to levodopa and a milder course without developing dementia. In addition, six of our 11 (54.5%) *SNCA* duplication patients had visual hallucinations including five in whom they occurred within 10 years of disease duration. PDD patients have a higher prevalence of hallucinations and delusions (45–65%) than PD patients (25%).[28,29] The prevalence of visual hallucination in our patients with *SNCA* duplication was similar to that of PDD patients. Interestingly, progressive myoclonus epilepsy type 1 (EPM1) is reported in the Lister family (17/1909 compared to the Swedish EPM prevalence of 1;20,000), however, only one of our patients (B-III-3) had a history of frontal lobe epilepsy without myoclonus.[30]

Remarkably three asymptomatic carriers were over 70 years of age without any signs of parkinsonism or dementia (Fig. 1 and supplementary Fig. 2). The calculated lifetime penetrance ratio was 43.8%. The same penetrance values (33–50%) have also been observed in Korean *SNCA* duplication pedigrees.[10] Before this study, we thought that asymptomatic carriers may already have pre-motor olfactory problems or sleep disorders, based on the Braak hypothesis; olfactory dysfunction or RBD are reported in early stage of PD.[31] However, none of the asymptomatic carriers studied demonstrated any motor or non-motor symptoms. These findings suggest that not only genetic factors but also environmental exposure, modifier genes, or aging influence the development of the disease in *SNCA* duplication individuals.

PET and SPECT studies in *SNCA* multiplication families have previously demonstrated severe reduction in striate uptake by [^{123}I]-FP-CIT SPECT or 6-[^{18}F]-fluorodopa PET in the Iowan and Korean families.[10,15] Of note, our patients with *SNCA* duplication showed severe reduction of the isotope signal in the caudate and anterior and posterior putamen by [^{11}C]-CFT PET, unlike our asymptomatic carriers and sporadic PD patients. This has not been observed in sporadic PD and may be a feature of *SNCA* multiplication disease, therefore it will be of interest to re-examine the other *SNCA* multiplication families for this phenomenon. According to FDG–PET study, the severe reduction in posterior cingulated cortex and the parieto-temporal cortex was reported in two patients with *SNCA* duplication from one family; both patients had visual hallucination. Their findings are similar to those of our four patients with *SNCA* duplication. Hypoperfusion or hypometabolism in the occipital association cortex on FDG–PET is frequently observed in patients with DLB.[32–34] In conclusion, PET studies on *SNCA* duplication patients show similarities with DLB, whereas that of asymptomatic carriers did not show any change.

Our study indicates that motor and non-motor symptoms in patients with *SNCA* duplication are heterogeneous. Asymptomatic carriers did not have any abnormalities both clinically and in examination of PET, olfactory test, and PSG, even at >70 years of age. These results suggest that in addition to copy number variation, other factors influence the development of symptoms in subjects with *SNCA* duplications.

Acknowledgments: This work was supported by grant-in-aid for scientific research on priority areas (research on pathomechanisms of brain disorders) from the MEXT of Japan (#20023028). K.N. was supported by a Eli-Lilly scholarship and a Herb Geist gift for Lewy body research. We would like to thank Hiroyo Yoshino and Yoko Imamichi (Juntendo University) for management of all DNA samples, Kazuyoshi Namba (Yoyogi sleep disorder clinic) for analyzing PSG, and Haruo Hanyu (Tokyo Medical University) for providing clinical information of Patient E-III-2.

REFERENCES

1. Spillantini MG, Schmidt ML, Lee VM, Trojanowski JQ, Jakes R, Goedert M. Alpha-synuclein in Lewy bodies. Nature 1997; 388:839–840.
2. Polymeropoulos MH, Lavedan C, Leroy E, et al. Mutation in the alpha-synuclein gene identified in families with Parkinson's disease. Science 1997;276:2045–2047.
3. Kruger R, Kuhn W, Muller T, et al. Ala30Pro mutation in the gene encoding alpha-synuclein in Parkinson's disease. Nat Genet 1998;18:106–108.
4. Zarranz JJ, Alegre J, Gomez-Esteban JC, et al. The new mutation, E46K, of alpha-synuclein causes Parkinson and Lewy body dementia. Ann Neurol 2004;55:164–173.
5. Singleton AB, Farrer M, Johnson J, et al. Alpha-synuclein locus triplication causes Parkinson's disease. Science 2003;302:841.
6. Farrer M, Kachergus J, Forno L, et al. Comparison of kindreds with parkinsonism and alpha-synuclein genomic multiplications. Ann Neurol 2004;55:174–179.
7. Fuchs J, Nilsson C, Kachergus J, et al. Phenotypic variation in a large Swedish pedigree due to SNCA duplication and triplication. Neurology 2007;68:916–922.
8. Ibanez P, Bonnet AM, Debarges B, et al. Causal relation between alpha-synuclein gene duplication and familial Parkinson's disease. Lancet 2004;364:1169–1171.
9. Chartier-Harlin MC, Kachergus J, Roumier C, et al. Alpha-synuclein locus duplication as a cause of familial Parkinson's disease. Lancet 2004;364:1167–1169.
10. Ahn TB, Kim SY, Kim JY, et al. Alpha-synuclein gene duplication is present in sporadic Parkinson disease. Neurology 2008;70:43–49.
11. Nishioka K, Hayashi S, Farrer MJ, et al. Clinical heterogeneity of alpha-synuclein gene duplication in Parkinson's disease. Ann Neurol 2006;59:298–309.
12. Ross OA, Braithwaite AT, Skipper LM, et al. Genomic investigation of alpha-synuclein multiplication and parkinsonism. Ann Neurol 2008;63:743–750.
13. Ikeuchi T, Kakita A, Shiga A, et al. Patients homozygous and heterozygous for SNCA duplication in a family with parkinsonism and dementia. Arch neurol 2008;65:514–519.

14. Obi T, Nishioka K, Ross OA, et al. Clinicopathologic study of a SNCA gene duplication patient with Parkinson disease and dementia. Neurology 2008;70:238–241.
15. Muenter MD, Forno LS, Hornykiewicz O, et al. Hereditary form of parkinsonism—dementia. Ann Neurol 1998;43:768–781.
16. Gwinn-Hardy K, Mehta ND, Farrer M, et al. Distinctive neuropathology revealed by alpha-synuclein antibodies in hereditary parkinsonism and dementia linked to chromosome 4p. Acta Neuropathol (Berl) 2000;99:663–672.
17. Hughes AJ, Daniel SE, Kilford L, Lees AJ. Accuracy of clinical diagnosis of idiopathic Parkinson's disease: a clinico-pathological study of 100 cases. J Neurol Neurosurg Psychiatry 1992;55:181–184.
18. Miller SA, Dykes DD, Polesky HF. A simple salting out procedure for extracting DNA from human nucleated cells. Nucleic Acids Res 1988;16:1215.
19. Ishibashi K, Ishii K, Oda K, Kawasaki K, Mizusawa H, Ishiwata K. Regional analysis of age-related decline in dopamine transporters and dopamine D2-like receptors in human striatum. Synapse 2009;63:282–290.
20. American Academy of Sleep Medicine. International classification of sleep disorders, revised: diagnostic and coding manual. Rochester, MN: American Academy of Sleep Medicine; 2001.
21. Rechtschaffen A, Kales A. A manual of standardized terminology, techniques and scoring system for sleep stages of human subjects, public health service. Washington, DC: U.S. Government Printing Office; 1968.
22. Lapierre O, Montplaisir J. Polysomnographic features of REM sleep behavior disorder: development of a scoring method. Neurology 1992;42:1371–1374.
23. Stiasny-Kolster K, Clever SC, Moller JC, Oertel WH, Mayer G. Olfactory dysfunction in patients with narcolepsy with and without REM sleep behaviour disorder. Brain 2007;130 (Part 2):442–449.
24. Katotomichelakis M, Balatsouras D, Tripsianis G, Tsaroucha A, Homsioglou E, Danielides V. Normative values of olfactory function testing using the "sniffin" sticks'. Laryngoscope 2007;117:114–120.
25. Hummel T, Sekinger B, Wolf SR, Pauli E, Kobal G. "Sniffin" sticks': olfactory performance assessed by the combined testing of odor identification, odor discrimination and olfactory threshold. Chem Senses 1997;22:39–52.
26. Iranzo A, Molinuevo JL, Santamaria J, et al. Rapid-eye-movement sleep behaviour disorder as an early marker for a neurodegenerative disorder: a descriptive study. Lancet Neurol 2006; 5:572–577.
27. Farrer MJ. Genetics of Parkinson disease: paradigm shifts and future prospects. Nat Rev Genet 2006;7:306–318.
28. Aarsland D, Ballard C, Larsen JP, McKeith I. A comparative study of psychiatric symptoms in dementia with Lewy bodies and Parkinson's disease with and without dementia. Int J Geriatr psychiatry 2001;16:528–536.
29. Emre M, Aarsland D, Brown R, et al. Clinical diagnostic criteria for dementia associated with Parkinson's disease. Mov Disord 2007;22:1689–1707; quiz1837.
30. Puschmann A, Wszolek ZK, Farrer M, Gustafson L, Widner H, Nilsson C. Alpha-synuclein multiplications with parkinsonism, dementia or progressive myoclonus? Parkinsonism Relat Disord 2009;15:390–392.
31. Braak H, Rub U, Gai WP, Del Tredici K. Idiopathic Parkinson's disease: possible routes by which vulnerable neuronal types may be subject to neuroinvasion by an unknown pathogen. J Neural Transm 2003;110:517–536.
32. Albin RL, Minoshima S, D'Amato CJ, Frey KA, Kuhl DA, Sima AA. Fluoro-deoxyglucose positron emission tomography in diffuse Lewy body disease. Neurology 1996;47:462–466.
33. Ishii K, Imamura T, Sasaki M, et al. Regional cerebral glucose metabolism in dementia with Lewy bodies and Alzheimer's disease. Neurology 1998;51:125–130.
34. Lobotesis K, Fenwick JD, Phipps A, et al. Occipital hypoperfusion on SPECT in dementia with Lewy bodies but not AD. Neurology 2001;56:643–649.

Journal of the Neurological Sciences xxx (2009) xxx–xxx

Contents lists available at ScienceDirect

Journal of the Neurological Sciences

journal homepage: www.elsevier.com/locate/jns

Comparison study of amyloid PET and voxel-based morphometry analysis in mild cognitive impairment and Alzheimer's disease

Masaaki Waragai [a], Nobuyuki Okamura [b,*], Katsutoshi Furukawa [a], Manabu Tashiro [c], Shozo Furumoto [b,d], Yoshihito Funaki [e], Motohisa Kato [b], Ren Iwata [e], Kazuhiko Yanai [b], Yukitsuka Kudo [f], Hiroyuki Arai [a]

[a] Department of Geriatrics and Gerontology, Division of Brain Sciences, Institute of Development, Aging and Cancer, Tohoku University, Sendai, Japan
[b] Department of Pharmacology, Tohoku University School of Medicine, Sendai, Japan
[c] Division of Cyclotron Nuclear Medicine, Cyclotron and Radioisotope Center, Tohoku University, Sendai, Japan
[d] Department of Nuclear Medicine and Radiology, Institute of Development, Aging and Cancer, Tohoku University, Sendai, Japan
[e] Division of Radiopharmaceutical Chemistry, Cyclotron and Radioisotope Center, Tohoku University, Sendai, Japan
[f] Innovation of New Biomedical Engineering Center, Tohoku University, Sendai, Japan

ARTICLE INFO

Article history:
Received 27 February 2009
Received in revised form 5 May 2009
Accepted 2 June 2009
Available online xxxx

Keywords:
Alzheimer's disease
Amyloid
Early diagnosis
Magnetic resonance imaging
Positron emission tomography
BF-227

ABSTRACT

Two techniques employed for the early diagnosis of dementia are the imaging of amyloid-β protein using positron emission tomography (PET) and voxel-based morphometry analysis of MRI (VBM–MRI). The purpose of this study was to evaluate the clinical utility of amyloid PET and VBM–MRI for the early diagnosis and tracking of the severity of Alzheimer's disease (AD). The neuritic plaque burden and gray matter losses were evaluated using [^{11}C]BF-227–PET and VBM–MRI in 12 healthy controls, 13 subjects with mild cognitive impairment (MCI), including 6 who converted to AD and 7 who did not convert, and 15 AD patients. The AD patients and the MCI converters exhibited a neocortical retention of BF-227 and parahippocampal gray matter loss shown by VBM–MRI. The MCI converters were more clearly distinguished from the MCI non-converters in BF-227–PET than VBM–MRI. The combined sample of the MCI converters and AD patients showed a significant correlation of MMSE scores with the global gray matter loss, but not with the BF-227 retention. These findings suggest that amyloid PET using [^{11}C]BF-227 is better suited for the prediction of conversion from MCI to AD, while VBM–MRI appears to be better suited for tracking the severity of dementia.

1. Introduction

Alzheimer's disease (AD) is a neurodegenerative disorder characterized by a progressive impairment of cognitive function and behavior. AD is the most common form of dementia, particularly in the elderly [1,2]. The pathological hallmarks of AD are extracellular amyloid-β protein deposits called senile plaques (SPs) and intracellular neurofibrillary tangles (NFTs), which occur together with selective neuronal and synaptic loss [3,4]. These changes are also associated with progressive neuronal loss and resultant cerebral atrophy [5]. The presence of both SPs and NFTs are prerequisites for a definitive diagnosis of AD, but more attention has been focused on the role of amyloid-β protein (Aβ) in the pathogenesis of AD. Although the mechanisms of development of AD have not been completely elucidated, Aβ is assumed to play a causal role in the pathology of AD.

In vivo imaging techniques that can non-invasively and reliably assess Aβ deposition are currently receiving considerable attention in the search for a method for early diagnosis of AD [6–11]. Pittsburgh Compound-B (PIB) is at present the most commonly used probe for Aβ and has been applied to the diagnosis of AD and several other neurological disorders [12–16]. For example, amnesic mild cognitive impairment (MCI) is currently considered a prodromal state of AD, though not all individuals with MCI will develop AD; MCI converters and non-converters are difficult to distinguish from a clinical and neuropsychological perspective. Analysis of PIB–PET images in MCI subjects revealed a bimodal distribution of PIB uptake in the neocortex. About two thirds of MCI cases showed neocortical retention of PIB similar in distribution (and sometimes in degree) to AD, while the other third of MCI cases showed no cortical retention, similar to normal individuals [15,17,18]. A previous PIB–PET study demonstrated higher PIB retention in MCI converters than in non-converters, suggesting the utility of amyloid imaging in the prediction of progression to dementia [18].

We have developed novel benzoxazole derivatives for in vivo imaging of amyloid [19–21]. One of these agents, 2-(2-[2-demethylaminothiazol-5-yl]ethenyl)-6-(2-[Fluoro]ethoxy)benzoxazole (BF-227), displayed a high binding affinity to Aβ fibrils, excellent brain uptake and specifically labels amyloid deposits in transgenic mice [20,22]. A clinical PET study using [^{11}C]BF-227 demonstrated higher retention of this tracer in the

* Corresponding author. Department of Pharmacology, Tohoku University School of Medicine, Tohoku University, 2-1 Seiryo-machi, Aoba-ku, Sendai 980-8575, Japan. Tel.: +81 22 717 8058; fax: +81 22 717 8060.
E-mail address: oka@mail.tains.tohoku.ac.jp (N. Okamura).

0022-510X/$ – see front matter © 2009 Elsevier B.V. All rights reserved.
doi:10.1016/j.jns.2009.06.005

Please cite this article as: Waragai M, et al, Comparison study of amyloid PET and voxel-based morphometry analysis in mild cognitive impairment and Alzheimer's disease, J Neurol Sci (2009), doi:10.1016/j.jns.2009.06.005

neocortex of AD patients than normal individuals [22]. There are several drawbacks to the use of this tracer, including its relatively low affinity to AD brain tissue ($K_d = 25$ nM) compared to PIB [23] and its slower clearance from the white matter region due to its higher lipophilicity (Log$P = 1.75$),[22] resulting in lower signal to background ratio than PIB–PET. However, the voxel-based analysis of BF-227–PET images indicated a pattern of tracer distribution distinct from that of PIB–PET.[12] Intriguingly, the preferential [^{11}C]BF-227 retention in the posterior neocortical region of the AD brain corresponded with an area containing a high density of neuritic plaques [4,22]. A preliminary report of the direct comparison of PIB–PET and BF-227–PET in the same AD patients additionally demonstrated a difference in the regional distribution of these two agents, which presumably reflects their different preference for various conformations of Aβ in the senile plaque generation process [24]. From these findings, we speculate that BF-227 detects neuritic plaques containing dense amyloid fibrils preferentially, compared to PIB–PET, and provides unique information about the Aβ pathology in AD patients. The early detection of Aβ deposition is important to begin medication to prevent a cognitive decline in the stage of MCI, since it appears that the deposition of Aβ starts earlier than the clinical diagnosis of dementia [25–27]. Approximately 20–30% of healthy, age-matched subjects exhibited neocortical retention of PIB, predominantly in the prefrontal and posterior cingulate cortices [15,16]. The demonstration of PIB retention in a proportion of normal individuals supports postmortem observations that Aβ aggregation predominantly occurs before the onset of dementia. However, there is currently no evidence that all PIB-positive normal individuals are destined to develop dementia. Highly sensitive detection of Aβ leads to a potential risk for misjudging the process of normal physiological aging as a pathological indicator of AD. The accurate prediction of AD progression is thus necessary to prevent the administration of non-essential treatments to individuals who are not at risk of converting to AD. In particular, a shift of brain Aβ from the soluble to fibrillar form is closely associated with onset of AD [28]. Thus, selective detection of dense amyloid fibrils would be advantageous to differentiate normal aging process from AD with high specificity, as the deposition of neuritic plaques is strongly associated with the earliest symptoms of AD [25]. Based on this background evidence, we anticipated that BF-227–PET would more accurately predict the conversion from MCI to AD than other imaging techniques.

Cognitive decline is reported to strongly correlate with cortical atrophy in AD, suggesting that cortical degeneration is the primary basis of cognitive decline in AD [5]. Thus, an increased rate of cerebral atrophy, as evaluated using MRI, is a diagnostic feature of AD that correlates with the clinical stage/severity and is thought to represent the macroscopic consequences of neuronal destruction [29–31]. Medial temporal lobe atrophy, as seen in MRI scans of AD patients, is a sensitive marker of AD even in its earliest stages. Volumetric analysis of the entorhinal cortex distinguished subjects who were destined to develop dementia from normal controls with high accuracy [32]. However, this approach is time-consuming and highly dependent on analyst expertise because it requires accurate manual outlining of the region of interest for the measurement. Voxel-based morphometry (VBM) has emerged as an ideal tool to visualize the changes in gray matter density in disease states. This technique has been reported to detect gray matter loss in MCI and AD patients. In addition, lower gray matter density has been reported in MCI converters compared with MCI non-converters [33–37]. These findings suggest that measurement of gray matter loss in the medial temporal lobe or the other regions might predict progression from MCI to AD with high accuracy. A direct comparison of MRI with PIB–PET was previously performed in the control, MCI and AD populations [38]. The distributions of hippocampal volume did not overlap between AD and normal control groups with the exception of one control subject, and MCI subjects are evenly distributed between the AD and normal controls. In contrast, PIB–PET uptake showed a bimodal distribution. While all AD subjects are tightly clustered in the high PIB retention range, both the normal control and MCI subjects segregate themselves into high and low PIB retention groups. The voxel-by-voxel comparisons of AD versus control patients revealed differences in the topographical distribution of amyloid deposition and in grey matter loss, suggesting that these two imaging strategies provide complementary information about AD pathology.

In this study, we performed amyloid-imaging PET using [^{11}C]BF-227 and VBM analysis of MRI images in subjects with MCI and AD. We investigated whether changes in BF-227 uptake and gray matter density were associated with later conversion to AD in MCI populations. Moreover, we examined the association of these measurements with cognitive function in AD and MCI converters to investigate whether these imaging strategies can track the severity of AD pathology.

2. Materials and methods

2.1. Staining of senile plaques using BF-227

Postmortem brain tissue from a 69-year-old male with autopsy-confirmed AD was obtained from Fukushimura Hospital (Toyohashi, Japan). Experiments were performed under the regulations of the hospital ethics committee. Serial sections (6 μm) taken from paraffin-embedded blocks of the temporal cortex were prepared in xylene and ethanol. Before BF-227 staining, quenching of autofluorescence was performed. The quenched tissue section was immersed in 100 μM of BF-227 containing 50% ethanol for 10 min. The section stained with BF-227 was then dipped briefly into water and rinsed in PBS for 60 min before coverslipping with FluorSave Reagent (Calbiochem, La Jolla, CA), and examined using an Eclipse E800 microscope (Nikon, Tokyo, Japan) equipped with a V-2A filter set (excitation 380–420 nm, dichroic mirror 430 nm, long pass filter 450 nm). An adjacent section was immunostained using a monoclonal antibody (mAb) against Aβ (6F/3D; Dako A/S, Glostrup, Denmark). After pretreatment with 90% formic acid for 5 min, sections were immersed in blocking solution for 30 min and then incubated for 60 min at 37 °C with 6F/3D at a dilution of 1:50. After incubation, sections were processed with the avidin–biotin method using a Pathostain ABC-POD(M) Kit (Wako, Osaka, Japan) and diaminobenzidine tetrahydrochloride.

2.2. Subjects

Patients recruited in the present study included 12 normal age-matched controls, 13 subjects with amnestic MCI, and 15 patients with AD. Diagnoses of probable AD were based on criteria from the National Institute of Neurological and Communicative Disorders and Stroke and the Alzheimer's Disease Related Disorders Association (NINCDS-ADRDA) [39]. The diagnosis of amnestic MCI was made according to the published criteria described previously [40]. All MCI subjects underwent medical and neuropsychological reevaluation at approximately 3 month intervals. Conversion to AD was diagnosed when (1) signs of deterioration of the general cognitive function were present and continued for at least 6 months, and (2) the patient's score on the Clinical Dementia Rating changed by more than 0.5 points. The MCI subjects were divided into two groups, MCI converters ($n = 6$) and MCI non-converters ($n = 7$). The MCI converters were defined as patients who eventually developed AD within a mean follow-up of 27.0 ± 7.9 months (range 14–30 months). The MCI non-converters were defined as having a transient memory loss or remaining cognitively stable through at least a 2 year follow-up (27.7 ± 2.2 months; range 25–30 months). The control group was recruited from volunteers who were not taking centrally-acting medications, had no cognitive impairment and had no cerebrovascular lesions identified via MRI. All subjects were screened using a questionnaire and medical history, and subjects with medical conditions potentially affecting the central nervous system were excluded. In addition, none

Please cite this article as: Waragai M, et al, Comparison study of amyloid PET and voxel-based morphometry analysis in mild cognitive impairment and Alzheimer's disease, J Neurol Sci (2009), doi:10.1016/j.jns.2009.06.005

Table 1
Demographic characteristics of the subjects.

	Control	MCI non-converter	MCI converter	AD
N	12	7	6	15
Age (year)	67.3 ± 2.7	77.6 ± 3.1	80.2 ± 4.1	71.0 ± 5.1
Gender (F/M)	6/6	2/5	4/2	8/7
MMSE	29.9 ± 0.3	26.3 ± 1.1	25.7 ± 2.0	19.8 ± 3.5

of the subjects had asymptomatic cerebral infarction detected via T2-weighted MRI. Demographic data for the subjects are shown in Table 1. Although the MCI converters and non-converters were statistically older than the control subjects and the AD patients, no statistical difference in age was observed between the MCI converters and the non-converters. The AD patients showed a significantly lower MMSE score than the MCI converters, non-converters, and control subjects ($p<0.05$), however, no statistical difference in MMSE score was observed between the MCI converters and the non-converters. The Committee on Clinical Investigation at Tohoku University School of Medicine and the Advisory Committee on Radioactive Substances at Tohoku University approved the study protocol.

3. MRI methods

All subjects underwent MRI with a 1.5 T MR scanner (GE Signa Hispeed, Milwaukee, WI). A three-dimensional volumetric acquisition of a T1-weighted gradient echo sequence produced a gapless series of thin axial sections using a vascular TOF SPGR sequence (echo time/repetition time, 2.4/50 ms; flip angle, 45°; acquisition matrix, 256×256; 1 excitation; field of view, 22 cm; slice thickness, 2.0 mm). Cerebral atrophy was evaluated by VBM [41]. For spatial normalization, a 12-parameter affine transformation was used to avoid segmentation errors caused by the partial-volume effects inherently created by warping. The normalized MRI was then segmented into gray matter, white matter, cerebrospinal fluid, and other components using SPM2 or SPM5 software. The segmentation procedure involved calculating the Bayesian probability of each voxel belonging to each tissue class based on a priori MRI information with a non-uniformity correction. The segmented gray matter images were then subjected to affine and non-linear spatial normalization using a template of a priori gray matter. The spatially normalized gray matter images were smoothed with an isotropic Gaussian kernel (12 mm at full width at half maximum) using the partial-volume effects to create a spectrum of gray matter intensities. The resulting gray matter intensities were equivalent to the weighted average of gray matter voxels located in the volume fixed by the smoothing kernel. Regional intensities can thus be considered equivalent to gray matter concentration. Differences of gray matter intensities between groups were assessed using a *t*-test with a height threshold of $p<0.05$, corrected for multiple comparisons by the family-wise error method. The extent threshold was set to 100 voxels. Parahippocampal gray matter density was additionally evaluated by calculating the average intensities in the bilateral parahippocampal region of interest (ROI) using Dr.View/LINUX software (AJS, Japan). To evaluate global atrophy, a *Z*-score map was created via the comparison of individual gray matter images with the mean and S.D. of gray matter images of healthy controls after voxel normalization to global mean intensities. The degree of global atrophy (% global atrophy) was calculated as a ratio of the area in which the *Z*-score of the voxel was more than 2.0 to whole brain area, using Voxel-Based Specific Regional Analysis System for AD (VSRAD) software (Eisai, Tokyo, Japan) [42].

3.1. PET procedure

Radiosynthesis of [^{11}C]BF-227 and the procedure used for BF-227–PET were performed as described previously. [22] BF-227 and its N-desmethylated derivative (a precursor of [^{11}C]BF-227) were custom-synthesized by Tanabe R&D Service Co. [^{11}C]BF-227 was synthesized from its precursor by N-methylation in dimethyl sulfoxide using [^{11}C]methyl triflate. The [^{11}C]BF-227–PET study was performed using a PET SET-2400W scanner (Shimadzu Inc., Japan). After an intravenous injection of 211–366 mBq [^{11}C]BF-227, dynamic PET images were obtained for 60 min with the subject's eyes closed. Standardized uptake value (SUV) images of [^{11}C]BF-227 were obtained by normalizing the tissue radioactivity concentration to the injected dose and body weight. ROIs were placed on individual axial MR images in the cerebellar hemisphere and the frontal, lateral temporal, parietal and posterior cingulate cortices. The ROI information was then copied onto the dynamic PET SUV images, and regional SUVs were sampled using Dr.View/LINUX software. The ratio of the regional to cerebellar SUV (SUVR) at 40–60 min post-injection was calculated, and averaged SUVR values in the frontal, temporal, parietal and posterior cingulate cortices were considered representative of BF-227 retention in the neocortex (neocortical SUVR).

3.2. Statistical analysis

Statistical comparison of PET and MRI measurements in the four groups was performed via an analysis of variance followed by a Bonferroni multiple comparisons test with a significance level of $p<0.05$. Statistical comparisons of age and MMSE scores in the four groups were performed using a Kruskal–Wallis test followed by a Dunn's multiple comparison test with a significance level of $p<0.05$. Correlations between the MMSE score and BF-227 retention in the neocortex or the cerebral atrophy index were examined using a non-parametric Spearman's rank correlation analysis. Correlations between the brain atrophy index and BF-227 retention were determined using Pearson's correlations. A linear model was applied to the data to obtain a correlation coefficient and *p* value. These analyses were performed using GraphPad Prism5 software (GraphPad, San Diego, CA).

4. Results

In order to confirm the selective binding ability of BF-227 to Aβ deposits, neuropathological examination was initially performed using BF-227 staining of AD temporal brain sections. Senile plaques were selectively stained with BF-227 and the staining pattern coincided well with Aβ immunostaining in an adjacent section (Fig. 1). Strikingly, cored plaques were intensely stained with BF-227, indicating preferential BF-227 binding to dense Aβ fibrils. Next,

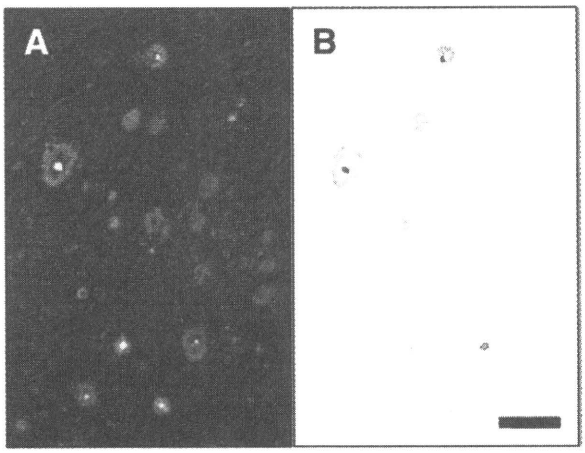

Fig. 1. (A) Neuropathological staining of human brain sections by BF-227. Amyloid plaques are clearly stained with BF-227 in AD temporal brain sections (B) BF-227 staining correlates well with Aβ immunostaining in adjacent sections. Scale bar = 100 μm.

Please cite this article as: Waragai M, et al, Comparison study of amyloid PET and voxel-based morphometry analysis in mild cognitive impairment and Alzheimer's disease, J Neurol Sci (2009), doi:10.1016/j.jns.2009.06.005

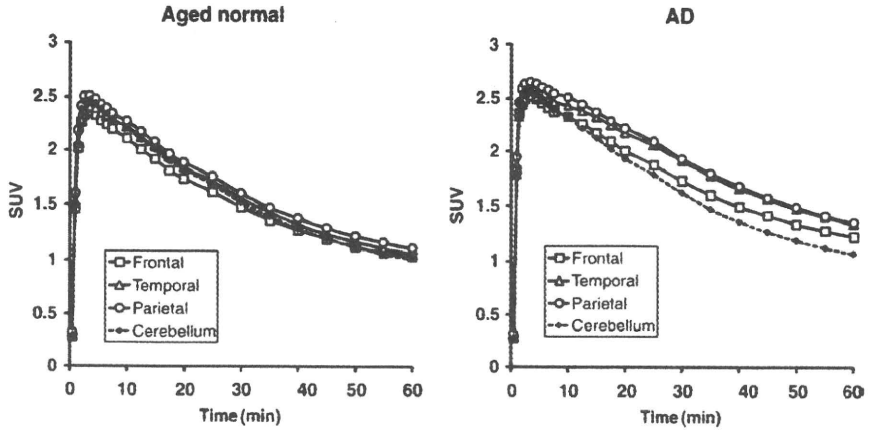

Fig. 2. Tissue time activity data for [^{11}C]BF-227–PET. SUV time activity curves of [^{11}C]BF-227 in the frontal cortex, lateral temporal cortex, parietal cortex and cerebellum are shown. Each point represents the mean of 12 control subjects (left) and 15 AD patients (right).

we performed clinical PET using [^{11}C]BF-227 in AD patients, MCI subjects and control subjects. The tissue time activity curves from [^{11}C]BF-227–PET in 15 AD patients and 12 normal controls are shown in Fig. 2. In AD patients, the frontal, temporal and parietal cortices retained [^{11}C]BF-227 to a greater extent at later time points, compared with controls. AD patients showed significantly higher SUVs in the temporal cortex and average neocortex than controls, but not in the cerebellum (Table 2). Therefore, neocortical SUV elevation in AD patients presumably reflects the specific binding of BF-227 to amyloid plaques. Representative images of [^{11}C]BF-227–PET and T1-weighted MRI in a normal control (70-year-old female, MMSE score 29), a MCI non-converter (76-year-old male, MMSE score 27), a MCI converter (85-year-old male, MMSE score 23), and an AD patient (62-year-old female, MMSE score 20) are shown in Fig. 3. Increased BF-227 retention was evident in both the MCI converter and the AD patient, but not in the control subject or the MCI non-converter. In AD patients, BF-227 SUVRs in the frontal, temporal, parietal and posterior cingulate cortices were significantly higher compared to the control subjects and the MCI non-converters (Table 2). A significant elevation of BF-227 SUVR was additionally observed in the frontal, temporal and parietal cortices of MCI converters compared with the control subjects. Consequently, the average neocortical SUVR was significantly higher in the AD patients and MCI converters than in normal subjects and MCI non-converters (Table 2). When a neocortical BF-227 SUVR of 1.11 (1.5SD above control mean) was used as a cut-off, sensitivity of 100% and a specificity of 91.7% in the discrimination between AD patients and normal subjects were achieved.

The voxel-based comparison of gray matter images using SPM5 demonstrated a significant decline of gray matter concentrations in the left ($-28, 14, -26, x, y, z$; $Z = 5.26$) and the right ($32, 18, -26, x, y, z$; $Z = 5.24$) medial temporal cortices of AD patients, compared with control subjects (Fig. 4A). SPM2 analysis using the same samples also showed a reduction of gray matter concentrations in nearly the same region and significance (data not shown). We drew the ROI in the parahippocampal area (Fig. 4B) and performed a comparison between the four groups. Significantly lower gray matter intensity was observed in the AD patients, MCI converters and MCI non-converters than in controls (Table 2, Fig. 5). However, age-related changes may be a confounding factor resulting in lower gray matter intensity in MCI groups, as MCI subjects were older than the normal control group. When a parahippocampal ROI value from SPM5 of 0.537 (2SD below control mean) was used as a cut-off, a sensitivity of 80.0% and a specificity of 100% were achieved in the discrimination between AD patients and normal subjects. No significant inter-group difference was observed in the percent global atrophy in VBM analysis due to substantial differences between individuals.

We focused on the comparison between the MCI converters and the non-converters, because these two populations showed no significant difference in age or MMSE scores. A significant inter-group difference was observed in the frontal and the average neocortical SUVR assayed by BF-227–PET, but not in the percent global atrophy or parahippocampal ROI value obtained by VBM–MRI (Table 2, Fig. 5). However, MCI converters showed a tendency toward lower parahippocampal ROI value derived from SPM5 than MCI non-converters.

Table 2
Summary of imaging measures.

	Normal	MCI non-converter	MCI converter	AD
BF-227 SUV in cerebellum	1.10 ± 0.19	1.08 ± 0.17	1.16 ± 0.22	1.16 ± 0.16
BF-227 SUV in frontal cortex	1.11 ± 0.19	1.10 ± 0.16	1.36 ± 0.33	1.31 ± 0.22
BF-227 SUV in temporal cortex	1.14 ± 0.19	1.19 ± 0.18	1.39 ± 0.28	1.45 ± 0.24[a]
BF-227 SUV in parietal cortex	1.20 ± 0.21	1.20 ± 0.18	1.38 ± 0.29	1.46 ± 0.23
BF-227 SUV in posterior cingulate cortex	1.22 ± 0.22	1.23 ± 0.22	1.39 ± 0.27	1.47 ± 0.21
Average neocortical BF-227 SUV	1.17 ± 0.20	1.18 ± 0.18	1.38 ± 0.29	1.42 ± 0.22[a]
BF-227 SUVR in frontal cortex	1.01 ± 0.06	1.02 ± 0.07	1.16 ± 0.10[a,b]	1.13 ± 0.08[a,b]
BF-227 SUVR in temporal cortex	1.04 ± 0.04	1.10 ± 0.07	1.20 ± 0.07[a]	1.24 ± 0.08[a,b]
BF-227 SUVR in parietal cortex	1.09 ± 0.04	1.12 ± 0.05	1.18 ± 0.07[a]	1.25 ± 0.08[a,b]
BF-227 SUVR in posterior cingulate cortex	1.11 ± 0.06	1.14 ± 0.07	1.20 ± 0.09	1.26 ± 0.05[a,b]
Average neocortical BF-227 SUVR	1.06 ± 0.04	1.09 ± 0.06	1.19 ± 0.07[a,b]	1.22 ± 0.06[a,b]
Percent global atrophy in VBM–MRI	4.24 ± 3.49	7.35 ± 5.94	5.96 ± 3.06	8.53 ± 4.44
Parahippocampal ROI value in VBM–MRI (SPM2)	0.642 ± 0.034	0.569 ± 0.039[a]	0.553 ± 0.044[a]	0.541 ± 0.055[a]
Parahippocampal ROI value in VBM–MRI (SPM5)	0.605 ± 0.034	0.510 ± 0.051[a]	0.473 ± 0.060[a]	0.475 ± 0.068[a]

[a] $p < 0.05$ vs. aged normal.
[b] $p < 0.05$ vs. MCI non-converter.

Please cite this article as: Waragai M, et al, Comparison study of amyloid PET and voxel-based morphometry analysis in mild cognitive impairment and Alzheimer's disease, J Neurol Sci (2009), doi:10.1016/j.jns.2009.06.005

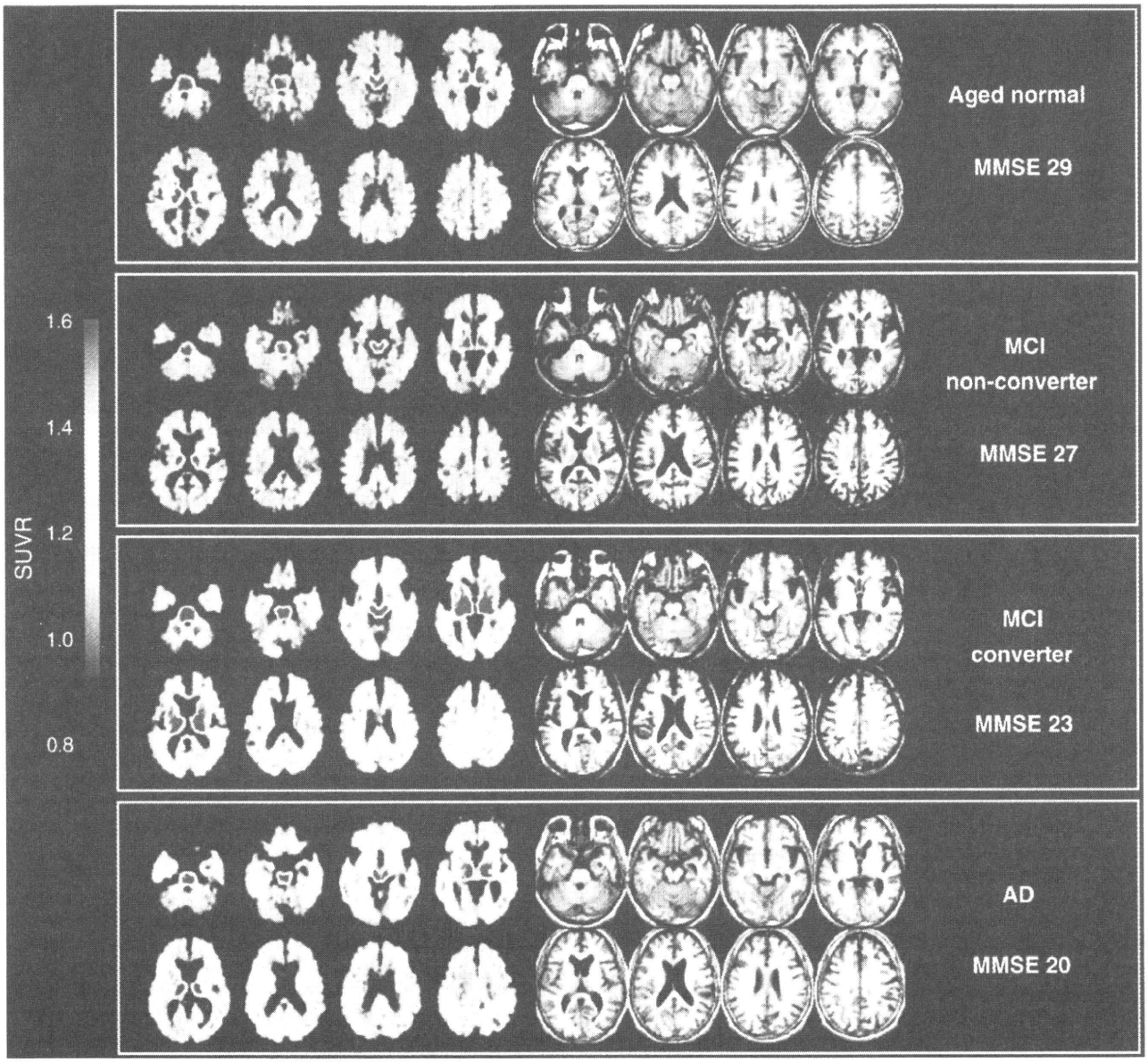

Fig. 3. Representative images of [^{11}C]BF-227-PET SUVR between 20 and 40 min post-injection (left) and T1-weighted MRI (right) in a control subject, a MCI non-converter, a MCI converter and an AD subject. The degree of [^{11}C]BF-227 retention is shown by color intensity from yellow to red in the cortex.

When we used a neocortical BF-227 SUVR of 1.11 as a cut-off, we achieved a sensitivity of 100% and a specificity of 71.4% in the discrimination between MCI converters and the MCI non-converters. These values were superior to the results of the parahippocampal ROI value derived from SPM5 (cut-off value: 0.537), which showed a sensitivity of 83.3% and a specificity of 42.9%. These data suggest that BF-227-PET is a better predictor of conversion from MCI to AD than VBM-MRI.

Next, we examined the correlations between MMSE scores and the three volume measurements (Fig. 6). When all subjects ($N=40$) were included in this analysis, a significant negative correlation was observed in all three measurements (BF-227 SUVR $r=-0.740$, $p<0.001$; percent global atrophy $r=-0.491$, $p=0.001$; parahippocampal ROI from SPM2 $r=0.674$, $p<0.001$; and parahippocampal ROI from SPM5 $r=0.687$, $p<0.001$). However, when we confined the analysis to the combined group of AD patients and MCI converters, we observed a significant correlation only between the percent global atrophy and the MMSE score (Spearman $r=-0.459$, $p=0.036$). In contrast, no significant correlation was observed between the parahippocampal ROI from SPM2 and the MMSE (Spearman $r=0.192$), between the parahippocampal ROI from SPM5 and the MMSE (Spearman $r=0.181$) or between the BF-227 SUVR in the neocortex and the MMSE (Spearman $r=-0.200$). Finally, no significant correlation was observed between the BF-227 SUVR and the percent global atrophy or parahippocampal atrophy in the analysis of all subjects.

5. Discussion

In the present study, MCI converters were more clearly distinguished from MCI non-converters by BF-227-PET than by VBM-MRI. The MCI non-converters showed a normal distribution of BF-227 except for one case, but also showed lower gray matter density in the parahippocampal gyrus than did normal controls. As a result, BF-227-PET achieved higher sensitivity and specificity in the discrimination between MCI converters and MCI non-converters than did VBM-MRI.

Please cite this article as: Waragai M, et al, Comparison study of amyloid PET and voxel-based morphometry analysis in mild cognitive impairment and Alzheimer's disease, J Neurol Sci (2009), doi:10.1016/j.jns.2009.06.005

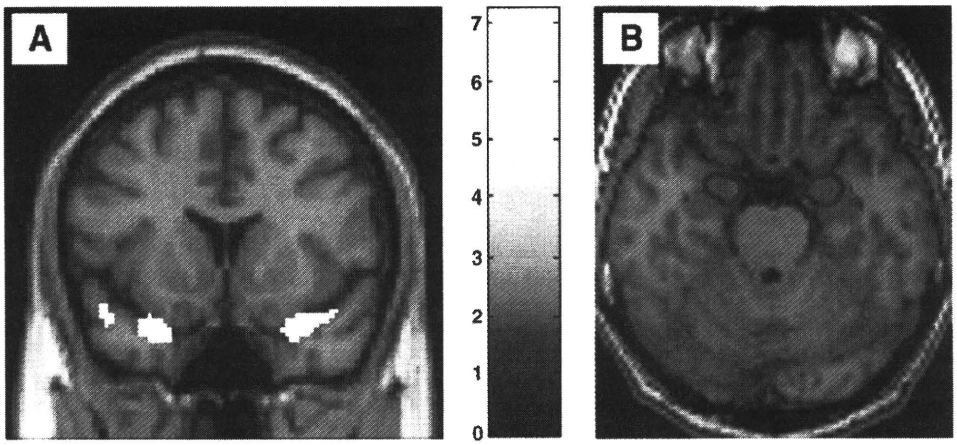

Fig. 4. (A) Areas of reduction in gray matter density of AD patients compared with aged normal controls. $p<0.05$, corrected for multiple comparisons. Left in the image is left in the brain. Color bars represent T values. (B) Regions of interest within the parahippocampal gyrus.

Our results strongly suggest that amyloid imaging using BF-227–PET will be a useful tool to predict conversion from MCI to AD, as previously shown for PIB–PET. [17,18] However, cerebral gray matter loss as determined by VBM–MRI was better correlated with the clinical severity of AD than BF-227–PET. Used together, BF-227–PET and VBM–MRI could be an effective method for the early diagnosis and severity tracking of AD. Our findings may be compatible with the theory that amyloid deposition reaches equilibrium or plateaus at an early stage of AD, making in vivo amyloid imaging useful in the examination of pre-symptomatic subjects [15,16]. Aβ deposition is a pathological hallmark of AD, but may also occur in normal elderly individuals who do not exhibit apparent cognitive decline. In fact, a PIB–PET study showed that 22% of healthy elderly individuals showed increased cortical PIB binding, indicating the presence of Aβ plaques in these non-symptomatic subjects [15]. A strong relationship between the impairment of episodic memory and PIB binding has also been shown both in subjects with MCI and in the normal population, suggesting that individuals with increased cortical PIB

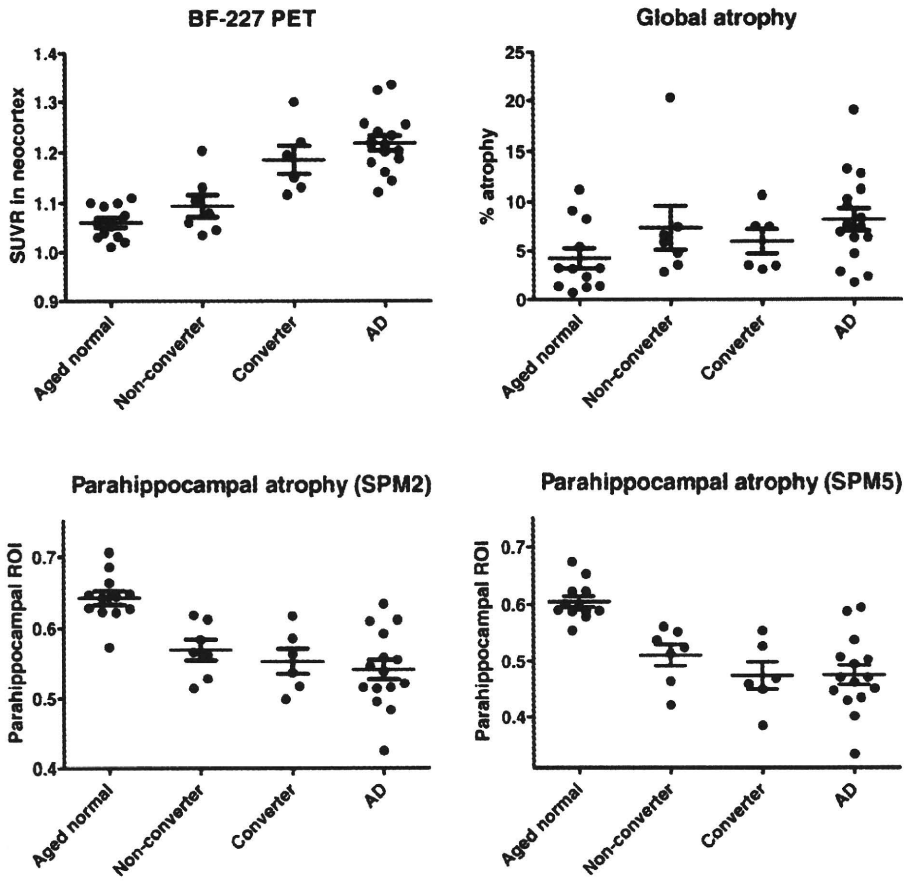

Fig. 5. Comparison of BF-227 SUVR in the neocortex (upper left), the percent global atrophy (upper right), the parahippocampal region of interest (ROI) value from gray matter images processed by SPM2 (lower left) and the parahippocampal ROI value from gray matter images processed by SPM5 (lower right) in control subjects, MCI non-converters, converters and AD patients.

Please cite this article as: Waragai M, et al, Comparison study of amyloid PET and voxel-based morphometry analysis in mild cognitive impairment and Alzheimer's disease, J Neurol Sci (2009), doi:10.1016/j.jns.2009.06.005

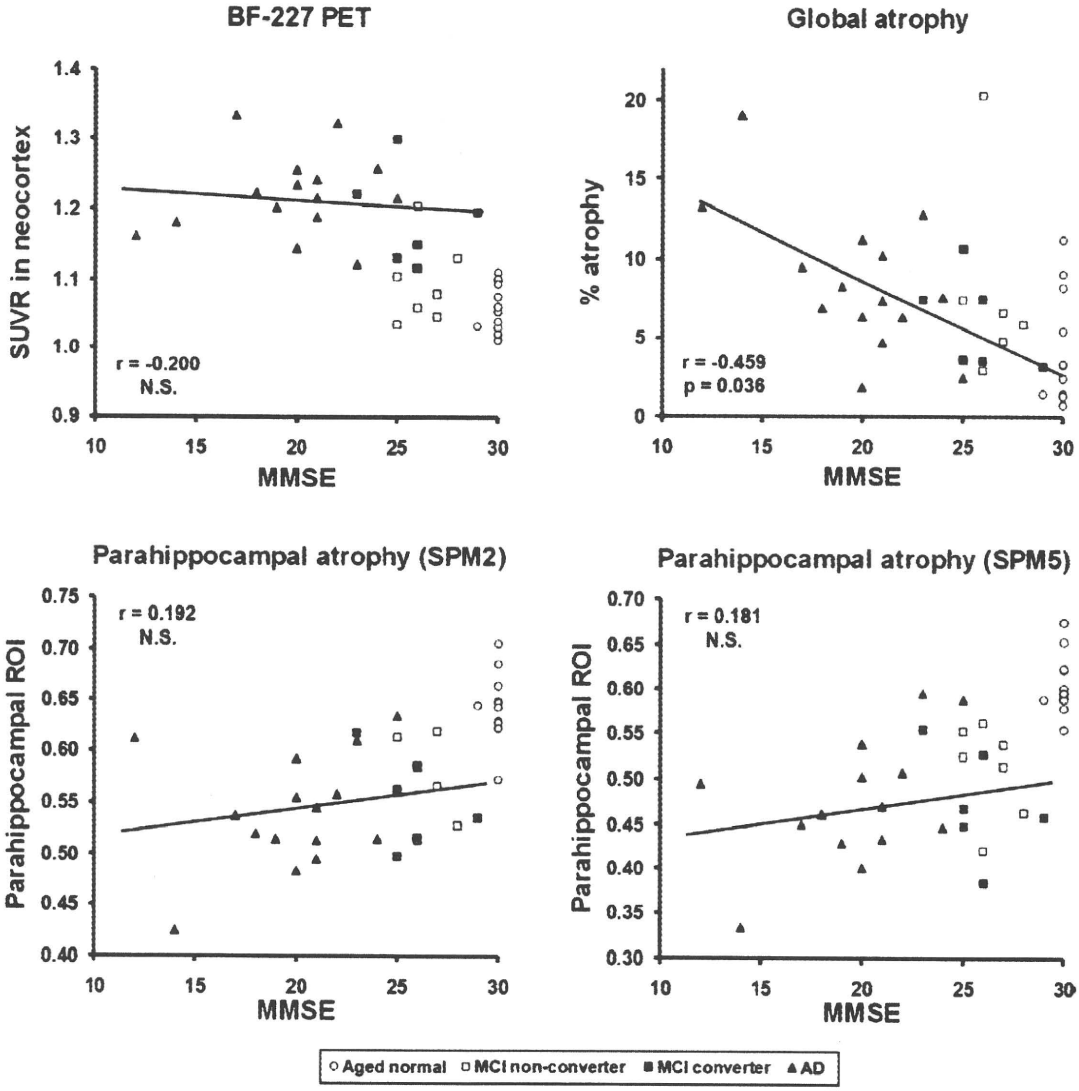

Fig. 6. The correlations of MMSE scores with the BF-227 SUVR in the neocortex (upper left), the percent global atrophy (upper right), the parahippocampal region of interest (ROI) value from gray matter images processed by SPM2 (lower left), and the parahippocampal ROI value from gray matter images processed by SPM5 (lower right). Open circle: control; open square: MCI non-converter; filled square: MCI converter; filled triangle: AD.

binding are proceeding to AD [43]. In our study, almost all normal subjects exhibited a normal distribution of BF-227 in the brain. This finding may suggest a lower sensitivity of diffuse amyloid plaque detection by BF-227 [22]. However, the proportion of amyloid PET-positive individuals in the normal population varies greatly depending on the characteristics of the sample population. Indeed, the mean age of the control subjects in our study was somewhat younger than in previous PIB–PET studies. Therefore, a direct comparison of BF-227–PET with PIB–PET in the same normal population is necessary to compare the ability of these agents to detect early AD pathology. A longitudinal follow-up of amyloid PET-positive cases in the healthy, normal population will also elucidate whether tracer uptake reflects pre-symptomatic detection of AD or a false-positive finding. A follow-up study of the patients with AD using PIB–PET showed that the amyloid deposition remains high but stable, despite decreases in regional glucose metabolism and cognitive function.[44] Our cross-sectional analysis also revealed a plateau of cortical BF-227 uptake in early AD patients, suggesting that amyloid formation reaches a plateau early in the course of AD. A potential limitation of this study is that it used a semiquantitative SUV measure to estimate BF-227 binding to amyloid plaques. The levels of neocortical BF-227 SUV might be underestimated due to hypoperfusion in AD patients. Quantitative analysis should be performed in future analyses to eliminate the influence of blood flow change.

A previous PIB–PET study found a positive correlation between the rate of whole brain atrophy and amyloid plaque load. [45] However, a recent PET study discovered a discrepancy between regional PIB retention and gray matter loss [38]. Additionally, histopathological analysis revealed no association between Aβ burden and brain atrophy [46]. The present study also found no significant correlation between neocortical BF-227 uptake and global gray matter loss in AD patients, in agreement with these findings. In our correlation analysis of the four measurements with the MMSE scores, we confined our analysis to AD patients and MCI converters because these patients share the same pathological process underlying AD. Therefore, this is more appropriate for the correlation analysis between cognitive function and the degree of Aβ burden or cerebral atrophy induced by the pathological process of AD than an analysis using all samples, including the normal population. In this analysis, the global gray matter loss measured by VBM–MRI was better correlated with MMSE scores than was the Aβ burden measured by BF-227–PET. A similar correlation analysis performed using PIB–PET demonstrated that the

Please cite this article as: Waragai M, et al, Comparison study of amyloid PET and voxel-based morphometry analysis in mild cognitive impairment and Alzheimer's disease, J Neurol Sci (2009), doi:10.1016/j.jns.2009.06.005

magnitudes of the correlations were greater for hippocampal atrophy than for neocortical PIB retention [38]. The current result, showing no significant correlation of the parahippocampal gray matter density with the MMSE score, seems to be inconsistent with previous PIB–PET data. We believe this discrepancy to be due mainly to differences in the sample population. The analysis in the previous PIB–PET study was performed using all the subjects, including the normal controls; our analysis was confined to AD patients and MCI converters who had already developed severe memory decline and probably substantial neuron loss in the hippocampus. These results suggest that global, rather than parahippocampal, gray matter loss is a potent indicator of dementia severity after the onset of memory loss in AD. We hope to explore the relationship between these imaging measurements and the impairment of episodic memory function in a future study.

It has been reported that the degree or rate of change of cerebral atrophy as measured by MRI analysis is closely related to the clinical progression of dementia [29,30]. Karas et al. performed a VBM–MRI analysis to examine the global and regional gray matter loss in normal, MCI and AD subjects, finding a significantly lower global gray matter volume in the AD subjects and an intermediate volume in the MCI subjects [31]. They followed the MCI subjects and observed greater gray matter loss in the MCI converters than in non-converters [37]. Another study also revealed different patterns of gray matter density distribution between MCI converters and non-converters [35]. From these findings, it appears that gray matter loss in VBM is a good indicator of conversion from MCI to AD. We failed to demonstrate significant inter-group differences between the MCI converters and non-converters, although the MCI converters showed a tendency toward lower parahippocampal gray matter density than did the non-converters. This, however, may be due to the small sample size and insufficient follow-up period (over two years) of the MCI subjects in this study. For example, one MCI non-converter in our study showed an abnormality in both the BF-227 SUVR and parahippocampal gray matter density; extending the follow-up period of the MCI subjects would likely result in more consistent correlation between MCI conversion to AD and the described measurements. Additional longitudinal studies are also needed to confirm the findings we have obtained and to examine the time course of AD, including changes in the pre-symptomatic subjects, and to determine the relationship between amyloid deposition and brain atrophy as underlying factors in the pathogenesis of AD.

Acknowledgements

We appreciate the technical assistance of Dr. S. Watanuki, Dr. Y. Ishikawa, Dr. M. Mori, and Dr. K. Sugi in the clinical PET studies and the support of Fukushimura Hospital for the histochemical studies. We also thank to Dr. H. Akatsu and Dr. T. Yamamoto for supplying brain samples. This study was supported by the Program for the Promotion of Fundamental Studies in Health Science of the National Institute of Biomedical Innovation, the Industrial Technology Research Grant Program in 2004 of the New Energy and Industrial Technology Development Organization (NEDO) of Japan, Health and Labor Sciences Research Grants for Translational Research from the Ministry of Health, an Asan Trazeneca Research Grant, and the Novartis Foundation for Gerontological Research.

References

[1] Blennow K, de Leon MJ, Zetterberg H. Alzheimer's disease. Lancet 2006;368: 387–403.
[2] Drachman DA. Aging of the brain, entropy, and Alzheimer disease. Neurology 2006;67:1340–52.
[3] Braak H, Braak E. Neuropathological stageing of Alzheimer-related changes. Acta Neuropathol 1991;82:239–59.
[4] Arnold SE, Hyman BT, Flory J, Damasio AR, Van Hoesen GW. The topographical and neuroanatomical distribution of neurofibrillary tangles and neuritic plaques in the cerebral cortex of patients with Alzheimer's disease. Cereb Cortex 1991;1:103–16.
[5] Mouton PR, Martin LJ, Calhoun ME, Dal Forno G, Price DL. Cognitive decline strongly correlates with cortical atrophy in Alzheimer's dementia. Neurobiol Aging 1998;19:371–7.
[6] Masters CL, Cappai R, Barnham KJ, Villemagne VL. Molecular mechanisms for Alzheimer's disease: implications for neuroimaging and therapeutics. J Neurochem 2006;97:1700–25.
[7] Nordberg A. PET imaging of amyloid in Alzheimer's disease. Lancet Neurol 2004;3: 519–27.
[8] Villemagne VL, Rowe CC, Macfarlane S, Novakovic KE, Masters CL. Imaginem oblivionis: the prospects of neuroimaging for early detection of Alzheimer's disease. J Clin Neurosci 2005;12:221–30.
[9] Mathis CA, Klunk WE, Price JC, DeKosky ST. Imaging technology for neurodegenerative diseases: progress toward detection of specific pathologies. Arch Neurol 2005;62:196–200.
[10] Nordberg A. Amyloid imaging in Alzheimer's disease. Curr Opin Neurol 2007;20: 398–402.
[11] Small GW, Kepe V, Ercoli LM, Siddarth P, Bookheimer SY, Miller KJ, et al. PET of brain amyloid and tau in mild cognitive impairment. N Engl J Med 2006;355:2652–63.
[12] Klunk WE, Engler H, Nordberg A, Wang Y, Blomqvist G, Holt DP, et al. Imaging brain amyloid in Alzheimer's disease with Pittsburgh Compound-B. Ann Neurol 2004;55:306–19.
[13] Price JC, Klunk WE, Lopresti BJ, Lu X, Hoge JA, Ziolko SK, et al. Kinetic modeling of amyloid binding in humans using PET imaging and Pittsburgh Compound-B. J Cereb Blood Flow Metab 2005;25:1528–47.
[14] Lopresti BJ, Klunk WE, Mathis CA, Hoge JA, Ziolko SK, Lu X, et al. Simplified quantification of Pittsburgh Compound B amyloid imaging PET studies: a comparative analysis. J Nucl Med 2005;46:1959–72.
[15] Rowe CC, Ng S, Ackermann U, Gong SJ, Pike K, Savage G, et al. Imaging beta-amyloid burden in aging and dementia. Neurology 2007;68:1718–25.
[16] Mintun MA, Larossa GN, Sheline YI, Dence CS, Lee SY, Mach RH, et al. [^{11}C]PIB in a nondemented population: potential antecedent marker of Alzheimer disease. Neurology 2006;67:446–52.
[17] Fripp J, Bourgeat P, Acosta O, Raniga P, Modat M, Pike KE, et al. Appearance modeling of ^{11}C PiB PET images: characterizing amyloid deposition in Alzheimer's disease, mild cognitive impairment and healthy aging. Neuroimage 2008;43:430–9.
[18] Forsberg A, Engler H, Almkvist O, Blomquist G, Hagman G, Wall A, et al. PET imaging of amyloid deposition in patients with mild cognitive impairment. Neurobiol Aging 2008;29:1456–65.
[19] Okamura N, Suemoto T, Shimadzu H, Suzuki M, Shiomitsu T, Akatsu H, et al. Styrylbenzoxazole derivatives for in vivo imaging of amyloid plaques in the brain. J Neurosci, 2004;24:2535–41.
[20] Okamura N, Furumoto S, Funaki Y, Suemoto T, Kato M, Ishikawa Y, et al. Binding and safety profile of novel benzoxazole derivative for in vivo imaging of amyloid deposits in Alzheimer's disease. Geriatr Gerontol Int 2007;7:393–400.
[21] Furumoto S, Okamura N, Iwata R, Yanai K, Arai H, Kudo Y. Recent advances in the development of amyloid imaging agents. Curr Top Med Chem 2007;7:1773–89.
[22] Kudo Y, Okamura N, Furumoto S, Tashiro M, Furukawa K, Maruyama M, et al. 2-(2-[2-Dimethylaminothiazol-5-yl]Ethenyl)-6-(2-[Fluoro]Ethoxy)Benzoxazole: A novel PET agent for in vivo detection of dense amyloid plaques in Alzheimer's disease patients. J Nucl Med 2007;48:553–61.
[23] Fodero-Tavoletti MT, Mulligan RS, Okamura N, Furumoto S, Rowe CC, Kudo Y, et al. In vitro characterization of BF227 binding to α-synuclein/Lewy Bodies. Eur J Pharmacol. (in press).
[24] Ishii K, Hashimoto M, Kimura Y, Sakata M, Oda K, Kawasaki K, et al. Direct comparison of in vivo accumulation of ^{11}C-PIB and ^{11}C-BF227 in Alzheimer's disease. Alzheimer's and Dementia, vol. 4, Issue 4; July 2008. p. T49. Supplement 1.
[25] Tiraboschi P, Hansen LA, Thal LJ, Corey-Bloom J. The importance of neuritic plaques and tangles to the development and evolution of AD. Neurology 2004;62:1984–9.
[26] Price JL, Morris JC. Tangles and plaques in nondemented aging and "preclinical" Alzheimer's disease. Ann Neurol 1999;45:358–68.
[27] Morris JC, Storandt M, Miller JP, McKeel DW, Price JL, Rubin EH, et al. Mild cognitive impairment represents early-stage Alzheimer disease. Arch Neurol 2001;58:397–405.
[28] Wang J, Dickson DW, Trojanowski JQ, Lee VM. The levels of soluble versus insoluble brain Abeta distinguish Alzheimer's disease from normal and pathologic aging. Exp Neurol 1999;158:328–37.
[29] Fox NC, Crum WR, Scahill RI, Stevens JM, Janssen JC, Rossor MN. Imaging of onset and progression of Alzheimer's disease with voxel-compression mapping of serial magnetic resonance images. Lancet 2001;358:201–5.
[30] Jack Jr CR, Shiung MM, Gunter JL, O'Brien PC, Weigand SD, Knopman DS, et al. Comparison of different MRI brain atrophy rate measures with clinical disease progression in AD. Neurology 2004;62:591–600.
[31] Karas GB, Scheltens P, Rombouts SA, Visser PJ, van Schijndel RA, Fox NC, et al. Global and local gray matter loss in mild cognitive impairment and Alzheimer's disease. Neuroimage 2004;23:708–16.
[32] Killiany RJ, Gomez-Isla T, Moss M, Kikinis R, Sandor T, Jolesz F, et al. Use of structural magnetic resonance imaging to predict who will get Alzheimer's disease. Ann Neurol 2000;47:430–9.
[33] Bell-McGinty S, Lopez OL, Meltzer CC, Scanlon JM, Whyte EM, Dekosky ST, et al. Differential cortical atrophy in subgroups of mild cognitive impairment. Arch Neurol 2005;62:1393–7.
[34] Chetelat G, Landeau B, Eustache F, Mezenge F, Viader F, de la Sayette V, et al. Using voxel-based morphometry to map the structural changes associated with rapid conversion in MCI: a longitudinal MRI study. Neuroimage 2005;27:934–46.
[35] Bozzali M, Filippi M, Magnani G, Cercignani M, Franceschi M, Schiatti E, et al. The contribution of voxel-based morphometry in staging patients with mild cognitive impairment. Neurology 2006;67:453–60.

Please cite this article as: Waragai M, et al, Comparison study of amyloid PET and voxel-based morphometry analysis in mild cognitive impairment and Alzheimer's disease, J Neurol Sci (2009), doi:10.1016/j.jns.2009.06.005

[36] Hämäläinen A, Tervo S, Grau-Olivares M, Niskanen E, Pennanen C, Huuskonen J, et al. Voxel-based morphometry to detect brain atrophy in progressive mild cognitive impairment. Neuroimage 2007;37:1122–31.
[37] Karas G, Sluimer J, Goekoop R, van der Flier W, Rombouts SA, Vrenken H, et al. Amnestic mild cognitive impairment: structural MR imaging findings predictive of conversion to Alzheimer disease. Am J Neuroradiol 2008;29:944–9.
[38] Jack Jr CR, Lowe VJ, Senjem ML, Weigand SD, Kemp BJ, Shiung MM, et al. ^{11}C PiB and structural MRI provide complementary information in imaging of Alzheimer's disease and amnestic mild cognitive impairment. Brain 2008;131:665–80.
[39] McKhann G, Drachman D, Folstein M, Katzman R, Price D, Stadlan EM. Clinical diagnosis of Alzheimer's disease: report of the NINCDS-ADRDA Work Group under the auspices of Department of Health and Human Services Task Force on Alzheimer's Disease. Neurology 1984;34:939–44.
[40] Petersen RC, Smith GE, Waring SC, Ivnik RJ, Tangalos EG, Kokmen E. Mild cognitive impairment: clinical characterization and outcome. Arch Neurol 1999;56:303–8.
[41] Ashburner J, Friston KJ. Voxel-based morphometry—the methods. Neuroimage 2000;11:805–21.
[42] Hirata Y, Matsuda H, Nemoto K, Ohnishi T, Hirao K, Yamashita F, et al. Voxel-based morphometry to discriminate early Alzheimer's disease from controls. Neurosci Lett 2005;382:269–74.
[43] Pike KE, Savage G, Villemagne VL, Ng S, Moss SA, Maruff P, et al. Beta-amyloid imaging and memory in non-demented individuals: evidence for preclinical Alzheimer's disease. Brain 2007;130:2837–44.
[44] Engler H, Forsberg A, Almkvist O, Blomquist G, Larsson E, Savitcheva I, et al. Two-year follow-up of amyloid deposition in patients with Alzheimer's disease. Brain 2006;129:2856–66.
[45] Archer HA, Edison P, Brooks DJ, Barnes J, Frost C, Yeatman T, et al. Amyloid load and cerebral atrophy in Alzheimer's disease: an ^{11}C-PIB positron emission tomography study. Ann Neurol 2006;60:145–7.
[46] Josephs KA, Whitwell JL, Ahmed Z, Shiung MM, Weigand SD, Knopman DS, et al. Beta-amyloid burden is not associated with rates of brain atrophy. Ann Neurol 2008;63:204–12.

Please cite this article as: Waragai M, et al, Comparison study of amyloid PET and voxel-based morphometry analysis in mild cognitive impairment and Alzheimer's disease, J Neurol Sci (2009), doi:10.1016/j.jns.2009.06.005

Altered Brain Serotonin Transporter and Associated Glucose Metabolism in Alzheimer Disease

Yasuomi Ouchi[1,2], Etsuji Yoshikawa[3], Masami Futatsubashi[3], Shunsuke Yagi[1], Takatoshi Ueki[4], and Kazuhiko Nakamura[5]

[1]Molecular Imaging Frontier Research Center, Hamamatsu University School of Medicine, Higashi-ku, Hamamatsu, Japan; [2]Positron Medical Center, Hamamatsu Medical Center, Hamakita-ku, Hamamatsu, Japan; [3]Central Research Laboratory, Hamamatsu Photonics K.K., Hamakita-ku, Hamamatsu, Japan; [4]Department of Neuroanatomy, Hamamatsu University School of Medicine, Higashi-ku, Hamamatsu, Japan; and [5]Department of Psychiatry, Hamamatsu University School of Medicine, Higashi-ku, Hamamatsu, Japan

Whether preclinical depression is one of the pathophysiologic features of Alzheimer disease (AD) has been under debate. In vivo molecular imaging helps clarify this kind of issue. Here, we examined in vivo changes in the brain serotoninergic system and glucose metabolism by scanning early- to moderate-stage AD patients with and without depression using PET with a radiotracer for the serotonin transporter, ^{11}C-3-amino-4-(2-dimethylaminomethylphenylsulfanyl) benzonitrile (DASB), and a metabolic marker, ^{18}F-FDG. **Methods:** Fifteen AD patients (8 nondepressed and 7 depressed) and 10 healthy subjects participated. All participants underwent 3-dimensional MRI and quantitative ^{11}C-DASB PET measurements, followed by ^{18}F-FDG PET scans in the AD group. Region-of-interest analysis was used to examine changes in ^{11}C-DASB binding potential estimated quantitatively by the Logan plot method in the serotonergic projection region. In addition, statistical parametric mapping was used to examine whether glucose metabolism in any brain region correlated with levels of ^{11}C-DASB binding in the dense serotonergic projection region (striatum) in AD. **Results:** Psychologic evaluation showed that general cognitive function (Mini-Mental State Examination) was similar between the 2 AD subgroups. Striatal ^{11}C-DASB binding was significantly lower in AD patients, irrespective of depression, than in healthy controls ($P < 0.05$, corrected), and ^{11}C-DASB binding in other dense projection areas decreased significantly in the depressive group, compared with the control group. The ^{11}C-DASB binding potential levels in the subcortical serotonergic projection region correlated negatively with depression score (Spearman correlation, $P < 0.01$) but not with dementia score. Statistical parametric mapping correlation analysis showed that glucose metabolism in the right dorsolateral prefrontal cortex was positively associated with the level of striatal ^{11}C-DASB binding in AD. **Conclusion:** The significant reduction in ^{11}C-DASB binding in nondepressed AD patients suggests that presynaptic serotonergic function is altered before the development of psychiatric problems such as depression in AD. The depressive AD group showed greater and broader reductions in binding, suggesting that a greater loss of serotonergic function relates to more severe psychiatric symptoms in the disease. This serotonergic dysfunction may affect the activity of the right dorsolateral prefrontal cortex, a higher center of cognition and emotion in AD.

Key Words: Alzheimer's disease; serotonin transporter; glucose metabolism; depression; positron emission tomography

J Nucl Med 2009; 50:1260–1266
DOI: 10.2967/jnumed.109.063008

Alzheimer disease (AD) is a neurodegenerative disorder with progressive memory and cognitive deterioration followed by or concomitant with psychologic problems such as depression and hallucination, which have a strong negative impact on the course of the disease. The occurrence of these psychologic disturbances has been reported to closely relate to disruption of the serotonergic system (*1*). Loss of neurons in the serotonergic raphe nuclei (*2*) and dysfunction of its nerve terminals in the neocortex (*3*) have been reported in AD. Many lines of evidence support this serotonin (5HT) deficiency theory concerning the psychobehavioral symptomatology of AD, as examined in postmortem (*4–6*) and pharmacotherapeutic (*7,8*) studies. A caveat of the postmortem studies is that the findings do not always reflect the antemortem conditions of AD because of variations of clinical symptoms after a mixture of nootropic and psychiatric drugs administered during the patient's lifetime. In addition, the comorbidity of intrinsic depression in patients with AD may be a confounding factor in a study of in vivo serotonergic changes in AD. In vivo studies using PET so far have focused on 5HT receptors in the limbic brain region in association with mnemonic cognitive impairment in AD (*9–11*). Thus, the alterations in presynaptic 5HT function relative to psychologic and behavioral problems in AD with and without depression remain to be investigated.

Received Feb. 9, 2009; revision accepted Apr. 2, 2009.
For correspondence or reprints contact: Yasuomi Ouchi, Laboratory of Human Imaging Research, Molecular Imaging Frontier Research Center, Hamamatsu University School of Medicine, 1-20-1 Handayama, Higashi-ku, Hamamatsu 431-3192, Japan.
E-mail: ouchi@hama-med.ac.jp

The serotonergic projections from the dorsal raphe nucleus are dense in the basal ganglia and thalamus (*12,13*). The 5HT transporter is a component of 5HT presynaptic neurons and a therapeutic target of selective 5HT reuptake inhibitors, which are presently the first-choice treatment for AD patients with depression (*1*). Because the 5HT transporter located on the presynaptic 5HT terminal regulates 5HT signaling, levels of ^{11}C-3-amino-4-(2-dimethylaminomethylphenylsulfanyl) benzonitrile (DASB) binding in these regions reflect the activity of the presynaptic 5HT neurons chiefly in the dorsal raphe nuclei. A recent postmortem study showed a marked reduction in the binding of 5HT transporter tracer in the prefrontal cortex regardless of the presence of depression in AD (*14*). This finding suggests that the loss of raphe nuclei neurons and cortical 5HT transporter is one of the pathologic features of AD at the time of death. In addition, a recent SPECT study on AD with depression showed significantly lower perfusion in the dorsolateral prefrontal cortex (DLPFC) in patients with depressive symptoms than in patients without such symptoms (*15*). The DLPFC is known as a neural substrate of executive function that is consistently compromised in depression (*16*). Furthermore, patients with frontal glucose hypometabolism exhibit a faster deterioration of cognitive abilities (*17*) than do patients with glucose hypometabolism only in the posterior brain. Thus, a combination study of the presynaptic 5HT system and cerebral cortical metabolism is important in elucidating the underlying mechanism for AD with psychotic deterioration.

For this purpose, we measured 2 biomarkers on the same day in mild- to moderate-stage AD patients with and without depression to investigate the levels of presynaptic serotonergic function and cortical neuronal activity using PET with ^{11}C-DASB, a specific 5HT transporter marker, and ^{18}F-FDG.

MATERIALS AND METHODS

Participants

A total of 15 nootropic- and antipsychotic-naïve patients with AD (8 men, 7 women; mean age ± SD, 61.3 ± 5.9 y) and 10 age-, sex-, and education-matched healthy control subjects (5 men, 5 women; mean age, 55.8 ± 8.8 y) participated in the study. The diagnosis of AD was based on the criteria of the National Institute of Neurologic and Communicative Disorders and Stroke and the Alzheimer Disease and Related Disorders Association. The clinical dementia rating in all patients ranged from 1.0 to 1.5, and no patient had psychiatric disorders before the onset of dementia. The participants were evaluated with the Mini-Mental State Examination, the affect test for emotional cognition (subjects evaluate facial expressions on different cards by choosing appropriate answers from the basic emotions: happiness, sadness, surprise, disgust, anger, fear; the full score = 20) (*18*), and the geriatric depression scale (GDS, maximum = 15) for AD patients (*19*). AD patients were classified into 2 subgroups (nondepressed and depressed) according to the GDS scores as shown in Table 1. The present study was approved by the local Ethics Committee of the Hamamatsu University School of Medicine, and written informed consent was obtained from all participants themselves. We obtained written approval from the spouses or family members of AD patients as well.

MRI and PET Procedure

All participants first underwent 3-dimensional MRI just before the PET measurement. We used a static magnet (0.3 T MRP7000AD; Hitachi) with 3-dimensional mode sampling to determine the brain areas for setting the regions of interest (ROIs). The MRI measurements and a mobile PET gantry allowed us to reconstruct PET images parallel to the intercommisural line without reslicing. Using this approach, we were able to allocate ROIs to the target regions of the original PET images (*20*).

PET was performed as described previously (*20*) on a high-resolution brain SHR12000 tomograph (Hamamatsu Photonics K.K.) having an intrinsic resolution of 2.9 × 2.9 × 3.4 mm in full width at half maximum, 47 slices, and a 163-mm axial field of view. After head fixation using a thermoplastic face mask and a 10-min transmission scan for attenuation correction, serial scanning (4 × 30 s, 20 × 60 s, and 14 × 300 s) with periodic arterial blood sampling was performed for 92 min after a slow bolus injection (taking 1 min) of a 300-MBq dose of ^{11}C-DASB with a specific activity of more than 90 GBq/μmol. The method was the same as described previously for another 5HT transporter tracer, ^{11}C-McN5652 (*21*). After completion of the ^{11}C-DASB measurement (after 5 times the half-life of ^{11}C had elapsed), 10 min of emission data were acquired under resting conditions 50 min after

TABLE 1. Clinical Demographics

Category	AD (8 men, 7 women)		Control
	Nondepressed (4 men, 4 women)	Depressed (4 men, 3 women)	(5 men, 5 women)
Age (y)	62.3 (6.4)	60.1 (5.4)	55.8 (8.8)
Education (y)	13.6 (2.2)	14.8 (2.8)	14.0 (2.1)
Disease duration (y)	2.2 (1.5)	1.8 (0.9)	—
Mini-Mental State Examination score	18.9 (3.8)*	17.4 (3.8)*	29.2 (0.8)
Affect test score	12.7 (3.6)*	9.4 (3.7)*†	19.0 (1.1)
GDS score	1.6 (0.8)	8.4 (1.1)*†	0.6 (0.7)

*$P < 0.01$ (paired t test) vs. control.
†$P < 0.01$ vs. nondepressed AD group.
Data are mean values, with SD in parentheses.

injection of 90 MBq of ^{18}F-FDG, according to a previously described autoradiographic technique (*22*).

Image Data Analysis

To determine brain ROIs within the 5HT projection system, we used original morphologic MRI data instead of using spatially normalized MRI data. Most of the cell bodies are in the raphe nuclei in the midsagittal brain stem, with the largest collection of serotonergic neurons residing in the dorsal and median raphe nuclei of the caudal midbrain (*23*). The use of original MR images allowed us to demarcate ROIs on the region covering the substantia nigra (one of the 5HT projection area) on the MR image. In addition, multiple semicircular ROIs (~36–120 mm^2) were drawn bilaterally over the nucleus accumbens, thalamus, putamen, amygdala, prefrontal (Brodmann area 9) and temporal (Brodmann area 21) cortices, and cerebellum on the MR images in reference to an MRI atlas (*24*). These ROIs were then transferred onto the corresponding dynamic ^{11}C-DASB images with 6.8-mm slice-thickness data, generated after adding 2 consecutive slices using image-processing software (Dr View; Asahi Kasei Co.) on a workstation (Ultraspark 300; SUN Microsystems) (*20*).

In the ROI analysis, ^{11}C-DASB binding was quantified using a 2-tissue-compartment model, in which the cerebellar hemisphere was chosen as a reference region. The binding potential (BP) in each target region was calculated by the formula (target tissue Vd)/(cerebellum Vd) − 1, where each Vd (the volume of distribution) was obtained by the Logan graphical method (*25*). Because the pontine and medullary raphe nuclei send a proportion of 5HT axons into the cerebellum, this region is not an ideal candidate for a 5HT-free region. However, the use of the cerebellum as the reference region is acceptable in the present groups because smaller changes in the 5HT system were reported in the cerebellum (*26*).

In voxelwise analysis of ^{18}F-FDG data, all original PET data were converted into semiquantitative parametric images using a unit of standardized uptake denoting the tracer activity per injected dose normalized to body weight. Correlation analysis by statistical parametric mapping (SPM) was performed to examine neural correlates with the level of ^{11}C-DASB binding in the dense 5HT projection area—putamen in the AD group.

Statistics

First, right and left values for the ROIs in each region were averaged because no significant difference was observed between the interhemispheric values with the Student *t* test. Then, the regional ^{11}C-DASB BP values were compared among the 3 groups with 1-way ANOVA using a post hoc Student–Newman–Keuls test. Statistical significance was set at $P < 0.05$ because post hoc multiple comparisons were performed in the analyses. In addition, the Kendall τ test was performed to compare the regional ^{11}C-DASB BP values with the clinical variables in the AD group. The level of significance for the Kendall τ test was set at $P < 0.01$.

For the voxelwise mapping analysis, SPM software was used (SPM2; Wellcome Department of Cognitive Neurology). The standardized uptake value–based ^{18}F-FDG images were then smoothed with an isotropic gaussian kernel of an 8 × 8 × 8 mm filter, as described elsewhere (*27*). Voxel-based correlation between cerebral ^{18}F-FDG uptake and the ^{11}C-DASB BP in the dense 5HT projection area was computed by covariance analysis, using age as a confounding covariate. The statistical threshold was set at $P < 0.001$, and *P* values were left uncorrected.

RESULTS

Levels of ^{11}C-DASB Binding in the 3 Groups

One-way ANOVA showed that the levels of ^{11}C-DASB BP in the dense 5HT projection regions (midbrain, nucleus accumbens, putamen, and thalamus) of the depressed AD group and the level in the putamen of the nondepressed AD group were significantly lower than those in the control group (Table 2; Fig. 1). ^{11}C-DASB BP tended to be reduced in other dense projection areas of the 5HT system (nucleus accumbens, thalamus, and midbrain) in the nondepressed AD group. No significant reduction was found in the cortical areas of the AD group. No significant difference in ^{11}C-DASB binding was found between the nondepressed and depressed AD groups, although the depressed AD group showed a clear tendency toward lower levels. Representative ^{11}C-DASB PET images of subjects in each group are shown in Figure 1.

Correlation Between ^{11}C-DASB Binding and Clinical Parameters in AD Group

As shown in Figure 2A, the levels of ^{11}C-DASB BP in all dense 5HT projection regions correlated negatively with GDS scores (midbrain: $r = 0.692$, $P < 0.01$, $f(x) = -0.057x + 1.834$; putamen: $r = 0.72$, $P < 0.005$, $f(x) = -0.046x + 1.683$; thalamus: $r = 0.839$, $P < 0.005$, $f(x) = -0.046x + 1.638$), indicating that lower binding of ^{11}C-DASB in the 5HT system may be related to greater deterioration of the emotional state in AD. Although no significant correlation was found with the scores for dementia (Mini-Mental State Examination, Fig. 2B) or emotional cognition (affect test, Fig. 2C), there was a tendency toward positive correlations between the putaminal ^{11}C-DASB BP and the Mini-Mental State Examination scores and between subcortical ^{11}C-DASB BPs and the affect scores.

Neural Correlates of Cerebral Glucose Metabolism with Striatal ^{11}C-DASB Binding in AD Group

SPM correlation analysis showed that glucose metabolism in the right DLPFC and superior frontal gyrus corre-

TABLE 2. Levels of ^{11}C-DASB BP in the 3 Groups

	AD		
Brain region	Nondepressed	Depressed	Control
Midbrain	1.73 (0.32)	1.34 (0.15)*	2.01 (0.55)
Nucleus accumbens	1.18 (0.21)	1.03 (0.55)*	1.64 (0.37)
Putamen	1.54 (0.12)*	1.27 (0.25)*	2.05 (0.50)
Thalamus	1.64 (0.18)	1.35 (0.11)*	2.00 (0.23)
Amygdala	1.14 (0.32)	0.80 (0.31)	1.21 (0.34)
Prefrontal cortex	0.28 (0.11)	0.21 (0.08)	0.35 (0.18)
Temporal cortex	0.37 (0.10)	0.29 (0.09)	0.40 (0.11)

*$P < 0.05$ vs. control (Student–Newman–Keuls test).
Data are mean values, with SD in parentheses.

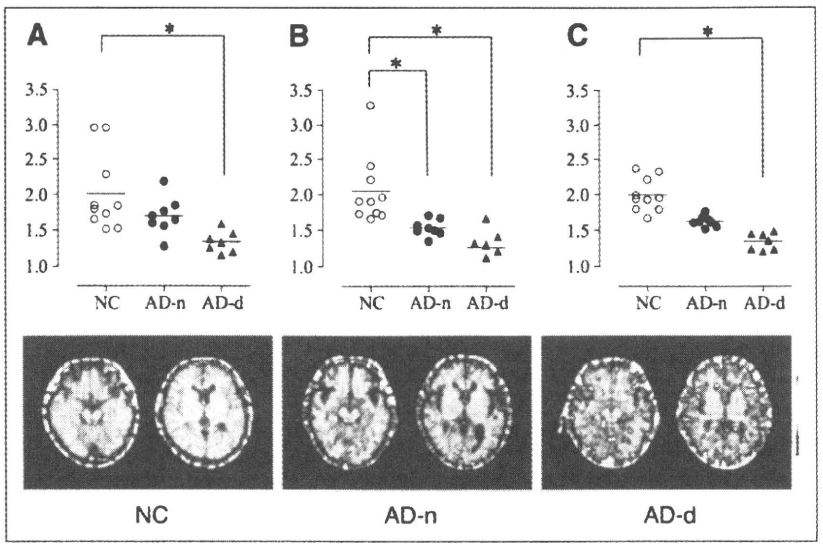

FIGURE 1. Levels of ^{11}C-DASB binding within dense 5HT projection areas in midbrain (A), putamen (B), and thalamus (C). Representative PET images of ^{11}C-DASB binding relative to cerebellar uptake are shown. Color scale denotes magnitude of tissue-to-cerebellum ratio, ranging from 0 to 3. NC = healthy control; AD-n = nondepressive AD; AD-d = depressive AD. *$P < 0.05$, ANOVA with post hoc Student–Newman–Keuls test.

lated positively with putaminal ^{11}C-DASB binding in AD patients (glass brain: Fig. 3A; Table 3). No other significant correlation was found, but there was a tendency toward a correlation when either ^{11}C-DASB BP in the thalamus or BP in the midbrain was chosen as a covariate (data not shown). The glucose metabolic level in the statistically highest peak region (right DLPFC) statistically correlated negatively with GDS scores in AD patients (Fig. 3B, scattergram, $r = 0.798$, $P < 0.0004$, $f(x) = -2.34x + 12.8$). Between-group comparison of SPM failed to show any brain region with statistically significant differences in glucose metabolism between the nondepressed and depressed groups (data not shown).

DISCUSSION

The present results showed a significant reduction in binding of the 5HT transporter marker ^{11}C-DASB in subcortical 5HT projection areas (especially the striatum) in patients with early- to moderate-stage AD regardless of depression and that the reduction was associated with the severity of their depressive states. The brain mapping analysis depicted the right DLPFC as a neural correlate of raphe-striatal 5HT activity in the disease. Furthermore, DLPFC metabolism was found to correlate with depressive scores, suggesting that 5HT dysfunction might affect right DLPFC activity, possibly leading to the generation of a clinical phenotype depression in AD. Thus, as suggested ex vivo (*3,28*), a progressive 5HT dysfunction may be present in the living brain of patients even in the absence of depression and may worsen the state of emotion.

In the present study, ^{11}C-DASB binding in the basal ganglia and thalamus in AD patients was about 25% that in healthy subjects—a smaller reduction than the loss of 5HT cell density observed in the raphe nucleus of postmortem AD brains (45%) (*29*). Although this difference might be due to differences between antemortem and postmortem specimens, a previous finding that marked 5HT cell attrition occurs regardless of the presence or absence of depression (*29*) and our finding that striatal ^{11}C-DASB binding is reduced in parallel with GDS scores suggest that 5HT neuronal reduction and psychologic deterioration may covary up to the last stage of 5HT neuronal loss in AD patients. Indeed, the 5HT neurons may be affected early in the course of the disease because AD patients with GDS scores of around zero showed a marked reduction in ^{11}C-DASB

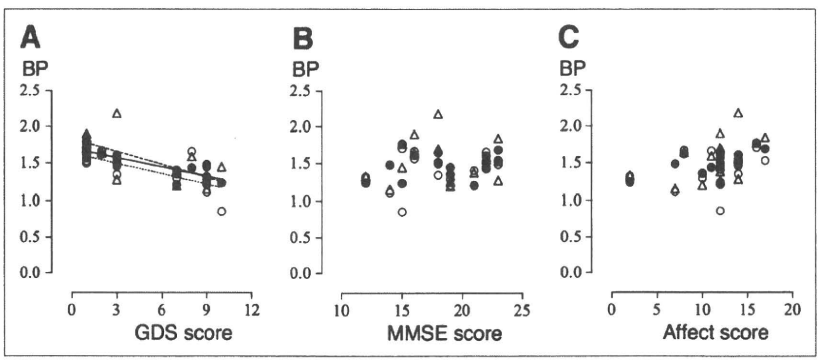

FIGURE 2. Correlations between levels of ^{11}C-DASB BP in midbrain (△), putamen (○), and thalamus (●) for GDS score (A), Mini-Mental State Examination (MMSE) score (B), and affect score (C) in all AD patients. Dotted (putamen), straight (thalamus), and dashed (midbrain) lines denote significant correlations (Kendall rank correlation, $P < 0.01$).

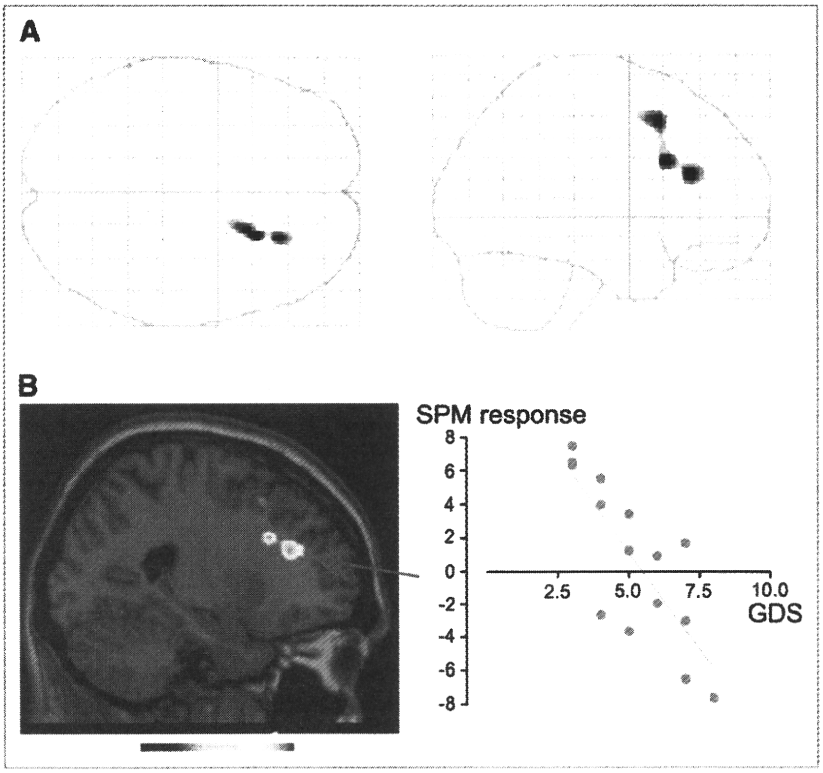

FIGURE 3. SPM images in AD group. (A) SPM correlation analysis showed positive correlation between striatal ^{11}C-DASB BP and glucose use in right DLPFC (glass brain, $P < 0.001$, uncorrected). (B) SPM responses in area with highest peak (arrow) correlated negatively with GDS scores. Color scale bar denotes *t* value.

binding specifically in the putamen, compared with that in healthy subjects (Fig. 1B). This finding is in contrast to the increase in binding of 5HT transporter marker ^{11}C-McN5652 in major depression, (*30*) suggesting that the underlying etiologies are clearly different. The mechanism of 5HT neuronal degeneration in AD remains unclear, but previous reports about the extent of 5HT neuron loss in the dorsomedial raphe nuclei (*28*) without association between 5HT transporter polymorphism and depression in depressed AD patients (*31*) suggest that the 5HT neuronal degeneration seems acquired. This may be true, because aggregation of Aβ protein exerts an early, focal neurotoxic effect on 5-HT and ACh axons (*32*).

It was reported that glucose metabolism in the DLPFC was lower in depressed AD patients than in their nondepressed counterparts (*33*). In the present study, we found a significant correlation between striatal ^{11}C-DASB binding and DLPFC glucose metabolism (Fig. 3A), the magnitude of which was associated with the extent of clinical deterioration and depression severity. Although striatal ^{11}C-DASB binding was lower in depressed AD patients in the present study, SPM analysis performed separately in each subgroup of AD (nondepressed and depressed) failed to show statistical significance for any brain region (data not shown). This result may be ascribed to the limited number of patients in each group or the narrow variation in ^{11}C-DASB BP in each subgroup. Previous studies showing that the DLPFC was involved in cognitive processing in negative emotion (*34*) and that successful 5HT augmentation therapy activated prefrontal glucose metabolism (*35*) would support our finding that striatal 5HT activity is associated with right DLPFC metabolism in AD patients. This right-

TABLE 3. Brain Regions Showing Significant Correlation Between Glucose Metabolism and Striatal ^{11}C-DASB Binding in AD

Brain region	Brodmann area	Coordinates			z score
		x	*y*	*z*	
Positive correlation					
Right DLPFC	9/46	22	22	28	3.91
Right superior frontal gyrus	8	20	16	48	3.79
Negative correlation (none)					

Height threshold, $P < 0.001$ (uncorrected); extent threshold, >100 voxels.

sided dominancy may reflect a depression-related susceptibility because lesions in the right frontal cortex lead to anxiety and depression (*36*) and because recent memories preferentially involve the right prefrontal cortex in AD (*37*). Thus, there might be a link between this important clinical phenomenon and a 5HT-related alteration in right prefrontal activity.

In the present study, no significant correlation was found between presynaptic 5HT dysfunction and dementia, whereas the scattergrams of Figures 2B and 2C showing a weak tendency toward a correlation may hint that a greater number of patients would exhibit significant correlations in presynaptic 5HT activity and these cognitive abilities. In addition, the limited number of clinical features in AD in the current study may be responsible for the failure in clinicobiochemical correlation. Previous reports showing that a reduction in 5HT signaling causes synaptic dysfunction and neuronal death in AD (*38*) and that enhanced 5HT signaling reduces levels of Aβ protein in the brain of transgenic AD mice (*39*) would support this speculation. At the moment, however, it is unlikely that the 5HT system is directly involved in the generation of dementia, as opposed to the implications of cholinergic failure in the AD brain. Because a history of depression is a risk factor of AD, alteration in the 5HT system even at an early stage of the disease should be borne in mind in the management of AD patients. Indeed, in the clinical setting, AD patients with neuropsychiatric symptoms tend to be institutionalized sooner than those without (*40*). Thus, on top of anticholinergic and antiamyloid deposition therapy, enhancement of 5HT signaling by, for example, selective 5HT reuptake inhibitors may be important in the treatment and prophylaxis of AD.

CONCLUSION

This study suggests that a degree of presynaptic 5HT function in the subcortical 5HT projection region is compromised in AD patients even before the development of depression. Right DLPFC dysfunction in parallel with 5HT inactivation is also implicated in the progression of emotional and cognitive deterioration in AD.

ACKNOWLEDGMENTS

We thank Dr. Mitsuo Kaneko (Kaneko Clinic), Dr. Masanobu Sakamoto (Hamamatsu Medical Center), Toshihiko Kanno (Hamamatsu Medical Center), and Yutaka Naito (Japan Environment Research Corporation) for their clinical and technical support. This work was supported by a Research Grant for Longevity Science from the Ministry of Health, Labor, and Welfare, Japan.

REFERENCES

1. Lanctôt KL, Herrmann N, Mazzotta P. Role of serotonin in the behavioral and psychological symptoms of dementia. *J Neuropsychiatry Clin Neurosci.* 2001; 13:5–21.
2. Mann DM, Yates PO. Serotonin nerve cells in Alzheimer's disease [letter]. *J Neurol Neurosurg Psychiatry.* 1983;46:96.
3. Palmer AM, Francis PT, Benton JS, et al. Presynaptic serotonergic dysfunction in patients with Alzheimer's disease. *J Neurochem.* 1987;48:8–15.
4. Assal F, Alarcón M, Solomon EC, Masterman D, Geschwind DH, Cummings JL. Association of the serotonin transporter and receptor gene polymorphisms in neuropsychiatric symptoms in Alzheimer disease. *Arch Neurol.* 2004;61:1249–1253.
5. Curcio CA, Kemper T. Nucleus raphe dorsalis in dementia of the Alzheimer type: neurofibrillary changes and neuronal packing density. *J Neuropathol Exp Neurol.* 1984;43:359–368.
6. Zubenko GS, Moossy J, Martinez AJ, et al. Neuropathologic and neurochemical correlates of psychosis in primary dementia. *Arch Neurol.* 1991;48:619–624.
7. Nyth AL, Gottfries CG. The clinical efficacy of citalopram in treatment of emotional disturbances in dementia disorders: a Nordic multicentre study. *Br J Psychiatry.* 1990;157:894–901.
8. Petracca G, Tesón A, Chemerinski E, Leiguarda R, Starkstein SE. A double-blind placebo-controlled study of clomipramine in depressed patients with Alzheimer's disease. *J Neuropsychiatry Clin Neurosci.* 1996;8:270–275.
9. Kepe V, Barrio JR, Huang SC, et al. Serotonin 1A receptors in the living brain of Alzheimer's disease patients. *Proc Natl Acad Sci USA.* 2006;103:702–707.
10. Meltzer CC, Smith G, DeKosky ST, et al. Serotonin in aging, late-life depression, and Alzheimer's disease: the emerging role of functional imaging. *Neuropsychopharmacology.* 1998;18:407–430.
11. Truchot L, Costes N, Zimmer L, et al. A distinct [^{18}F]MPPF PET profile in amnestic mild cognitive impairment compared to mild Alzheimer's disease. *Neuroimage.* 2008;40:1251–1256.
12. Lavoie B, Parent A. Immunohistochemical study of the serotoninergic innervation of the basal ganglia in the squirrel monkey. *J Comp Neurol.* 1990;299:1–16.
13. Lavoie B, Parent A. Serotoninergic innervation of the thalamus in the primate: an immunohistochemical study. *J Comp Neurol.* 1991;312:1–18.
14. Thomas AJ, Hendriksen M, Piggott M, et al. A study of the serotonin transporter in the prefrontal cortex in late-life depression and Alzheimer's disease with and without depression. *Neuropathol Appl Neurobiol.* 2006;32:296–303.
15. Levy-Cooperman N, Burhan AM, Rafi-Tari S, et al. Frontal lobe hypoperfusion and depressive symptoms in Alzheimer disease. *J Psychiatry Neurosci.* 2008;33:218–226.
16. Davidson RJ, Pizzagalli D, Nitschke JB, Putnam K. Depression: perspectives from affective neuroscience. *Annu Rev Psychol.* 2002;53:545–574.
17. Mann UM, Mohr E, Chase TN. Rapidly progressive Alzheimer's disease [letter]. *Lancet.* 1989;2:799.
18. Ouchi Y, Nakayama T, Kanno T, Yoshikawa E, Shinke T, Torizuka T. In vivo presynaptic and postsynaptic striatal dopamine functions in idiopathic normal pressure hydrocephalus. *J Cereb Blood Flow Metab.* 2007;27:803–810.
19. Weintraub D, Xie S, Karlawish J, Siderowf A. Differences in depression symptoms in patients with Alzheimer's and Parkinson's diseases: evidence from the 15-item Geriatric Depression Scale (GDS-15). *Int J Geriatr Psychiatry.* 2007;22:1025–1030.
20. Ouchi Y, Yoshikawa E, Okada H, et al. Alterations in binding site density of dopamine transporter in the striatum, orbitofrontal cortex, and amygdala in early Parkinson's disease: compartment analysis for beta-CFT binding with positron emission tomography. *Ann Neurol.* 1999;45:601–610.
21. Sekine Y, Ouchi Y, Takei N, et al. Brain serotonin transporter density and aggression in abstinent methamphetamine abusers. *Arch Gen Psychiatry.* 2006;63:90–100.
22. Phelps ME, Huang SC, Hoffman EJ, Selin C, Sokoloff L, Kuhl DE. Tomographic measurement of local cerebral glucose metabolic rate in humans with (F-18)2-fluoro-2-deoxy-D-glucose: validation of method. *Ann Neurol.* 1979;6:371–388.
23. Palacios JM, Waeber C, Hoyer D, Mengod G. Distribution of serotonin receptors. *Ann N Y Acad Sci.* 1990;600:36–52.
24. Mai JK, Assheuer J, Paxinos G. *Atlas of the Human Brain.* San Diego, CA: Academic Press; 1997.
25. Logan J, Volkow ND, Fowler JS, et al. Effects of blood flow on [^{11}C]raclopride binding in the brain: model simulations and kinetic analysis of PET data. *J Cereb Blood Flow Metab.* 1994;14:995–1010.
26. Procter AW, Lowe SL, Palmer AM, et al. Topographical distribution of neurochemical changes in Alzheimer's disease. *J Neurol Sci.* 1988;84:125–140.
27. Ouchi Y, Yoshikawa E, Futatsubashi M, Okada H, Torizuka T, Kaneko M. Activation in the premotor cortex during mental calculation in patients with Alzheimer's disease: relevance of reduction in posterior cingulate metabolism. *Neuroimage.* 2004;22:155–163.
28. Yamamoto T, Hirano A. Nucleus raphe dorsalis in Alzheimer's disease: neurofibrillary tangles and loss of large neurons. *Ann Neurol.* 1985;17:573–577.